The Effects of Small Amounts of H_2O, CO_2 and Na_2O on the Partial Melting of Spinel Lherzolite in the System CaO–MgO–Al$_2$O$_3$–SiO$_2$ ± H_2O ± CO_2 ± Na_2O at 1·1 GPa

XI LIU*, HUGH ST. C. O'NEILL† AND ANDREW J. BERRY

RESEARCH SCHOOL OF EARTH SCIENCES, AUSTRALIAN NATIONAL UNIVERSITY, CANBERRA, A.C.T. 0200, AUSTRALIA

The effects of small amounts of H_2O (<4 wt % in the melt) on the multiply saturated partial melting of spinel lherzolite in the system CaO–MgO–Al$_2$O$_3$–SiO$_2$ ± Na_2O ± CO_2 have been determined at 1·1 GPa in the piston-cylinder apparatus. Electron microprobe analysis and Fourier transform infrared spectroscopy were used to analyse the experimental products. The effects of H_2O are to decrease the melting temperature by 45°C per wt % H_2O in the melt, to increase the Al$_2$O$_3$ of the melts, decrease MgO and CaO, and leave SiO$_2$ approximately constant, with melts changing from olivine- to quartz-normative. The effects of CO_2 are insignificant at zero H_2O, but become noticeable as H_2O increases, tending to counteract the H_2O. The interaction between H_2O and CO_2 causes the solubility of CO_2 at vapour saturation to increase with increasing H_2O, for small amounts of H_2O. Neglect of the influence of CO_2 in some previous studies on the hydrous partial melting of natural peridotite may explain apparent inconsistencies between the results. The effect of small amounts of H_2O on multiply saturated melt compositions at 1·1 GPa is similar to that of K_2O, i.e. increasing H_2O or K_2O leads to quartz-normative compositions, but increasing Na_2O produces an almost opposite trend, towards nepheline-normative compositions.

KEY WORDS: H_2O; CO_2; FTIR; hydrous partial melting; mantle melting; spinel lherzolite; system CaO–MgO–Al$_2$O$_3$–SiO$_2$ ± H_2O ± CO_2 ± Na_2O

INTRODUCTION

H_2O and CO_2 are the most abundant and important magmatic volatile species (Bowen, 1928; Ingerson, 1960; Gill, 1981; Blank & Brooker, 1994; McMillan, 1994) and may have a strong influence on the generation of basaltic magma in the upper mantle (Yoder & Tilley, 1962; Kushiro, 1975, 1990; Ringwood, 1975; Gaetani & Grove, 1998; Green & Falloon, 1998; Schmidt & Poli, 1998; Ulmer, 2001; Dixon *et al.*, 2002; Asimow & Langmuir, 2003). The amount of H_2O in the hypothetical primitive mantle has been estimated at ~1160 ppm (O'Neill & Palme, 1998), but for real mantle peridotite it may range from ~200 ppm in the depleted mid-ocean ridge basalt (MORB)-source mantle to unconstrained higher values in the mantle wedge above subduction zones. The range of CO_2 in the mantle is about 230–550 ppm (Zhang & Zindler, 1993; Jambon, 1994).

A large number of experimental studies have been carried out to study the effect of H_2O on mantle melting relations, both in simplified analogue systems (Kushiro *et al.*, 1968a; Kushiro, 1969, 1972; Yoder, 1971) and with natural rock compositions (Kushiro *et al.*, 1968b, 1972; Nicholls & Ringwood, 1972, 1973; Green, 1973, 1976; Mysen & Boettcher, 1975a, 1975b; Kushiro, 1990; Hirose & Kawamoto, 1995; Hirose, 1997a; Gaetani & Grove, 1998; Muntener *et al.*, 2001). It is now rather clear that water substantially decreases the solidus temperature of natural peridotite, although this effect has not been well parameterized; as to its effect on the melt composition, however, there is still considerable disagreement. An earlier debate, on whether hydrous melting of peridotite produces andesitic or basaltic magma (Nicholls & Ringwood, 1972, 1973; Green, 1973; Mysen & Boettcher, 1975a, 1975b; Green, 1976),

*Present address: Geodynamics Research Center, Ehime University, Matsuyama 790-8577, Japan.
†Corresponding author. Telephone: (+61) 2 6125 5159. Fax: (+61) 2 6125 5989. E-mail: hugh.oneill@anu.edu.au

ended inconclusively. More recent experiments also show discrepancies (Kushiro, 1990; Hirose & Kawamoto, 1995; Hirose, 1997a; Gaetani & Grove, 1998; Muntener et al., 2001; Parman & Grove, 2004). The only thermodynamic analysis so far, performed by Gaetani & Grove (1998), indicated a positive correlation between the activity coefficient of SiO_2 and the H_2O content of the melt, which disagrees with a long-held opinion that depolymerization of silicate melts by the addition of H_2O should decrease the activity coefficient of SiO_2 (Warner, 1973; Kushiro, 1975; Stolper, 1982a).

In experiments in the simple systems enstatite (En)–H_2O (Kushiro et al., 1968a), forsterite (Fo)–diopside (Di)–En–H_2O (Kushiro, 1969), Fo–Di–silica (Qz)–H_2O (Kushiro, 1972) and Fo–nepheline (Ne)–Qz–H_2O (Kushiro, 1972), quartz-normative melts rather than olivine-normative melts were produced under water-saturated conditions at pressures up to at least 1·7 GPa. These results were taken to support the hypothesis that subduction-related andesites represent primary partial melts of hydrous mantle peridotite (O'Hara, 1965). It is now widely acknowledged that much of the ambiguity to do with the interpretation of experiments on the hydrous melting of peridotite is due to quench modification of melt compositions, but it should not be overlooked that such experiments may also suffer from other difficulties related to keeping the experimental charge closed to H_2O and to other volatile components, especially CO_2.

With only a few exceptions, most experiments on peridotite melting have been carried out either under nominally anhydrous or vapour-saturated conditions, or with H_2O controlled by an additional hydrous phase (amphibole or phlogopite), making the thermodynamic evaluation of the effects of intermediate amounts of water uncertain. Only relatively recently have experimental studies begun to address the question of the effects of small amounts of H_2O on partial melting in the mantle, including quantification of the amounts of H_2O in the melt (Gaetani & Grove, 1998; Falloon & Danyushevsky, 2000; Muntener et al., 2001; Pichavant et al., 2002). Various analytical methods have been used, namely Fourier transform infrared (FTIR) spectroscopy and secondary ionization mass spectrometry (SIMS), but also the 'by-difference' method with the electron microprobe, in which H_2O is estimated by the difference in the analytical total from 100 wt %, or direct analysis of O by electron microprobe analysis (EMPA) (so that only H is estimated 'by difference').

The effect of CO_2 on partial melting in peridotites has been less extensively studied than that of H_2O, either in simple systems or in natural compositions. Most experimental studies have focused on the petrogenesis of carbonatitic–kimberlitic magmas, in which the effects of CO_2 are obviously of primary importance (Mysen & Boettcher, 1975b; Wyllie & Huang, 1975, 1976; Mysen et al., 1976; Wyllie, 1977; Eggler, 1978; Eggler & Wendlandt, 1979; Green & Wallace, 1988; Wallace & Green, 1988; Falloon & Green, 1989; Ringwood et al., 1992; Dalton & Presnall, 1998a, 1998b). The solubility of CO_2 in silicate melts increases strongly with pressure [reviewed by Blank & Brooker (1994)], and therefore understandably most of the experimental studies listed above are at relatively high pressures, and mostly under vapour-saturated conditions. Experimental data at lower pressures pertinent to the genesis of MORB and island arc magmas are few.

Only a few studies have been carried out to assess the combined effects of H_2O and CO_2 even under vapour-saturated conditions (Mysen & Boettcher, 1975a, 1975b; Mysen, 1976; Taylor & Green, 1988, 1989). The only experimental study of mantle melting of which we are aware that reported both CO_2 and H_2O concentrations under vapour-absent conditions is the recent work of Gaetani & Grove (1998), in which CO_2 was observed as an accidental contaminant in the product melts and its influence was ignored.

It follows that an experimental study of partial melting of a simplified lherzolite phase assemblage in the system CaO–MgO–Al_2O_3–SiO_2–H_2O–CO_2 (CMAS–H_2O–CO_2) at relatively low pressure is highly desirable. It will create a link between experimental studies on anhydrous systems and vapour-saturated systems, thus potentially resolving some long-lasting controversies.

EXPERIMENTAL TECHNIQUES
Experimental strategy

The initial goal of this investigation was to determine the effects of adding H_2O only on the multiply saturated melting of spinel lherzolite (Fo + Sp + Opx + Cpx) in the system CMAS at 1·1 GPa. However, it proved impossible to eliminate CO_2 from our experiments, small amounts being observed in the FTIR spectra of all analysed runs, either from contamination of the starting material or by diffusion of C through the Pt capsules (Brooker et al., 1998). The study of Gaetani & Grove (1998), which addressed many of the same questions as this study, but in 'natural' (multicomponent) systems, reported the same problem. We also detected small amounts of Na_2O in the analyses of most glasses, because any Na_2O present in the chemicals used to prepare the starting materials becomes concentrated in the melt during the experiments. Accordingly, we decided to expand the scope of the investigation to address also the effects of CO_2 and Na_2O, so that by deliberately varying the quantities of these impurities we could deconvolute their effects from those of H_2O. Because CO_2 and Na_2O are of course important in natural systems, this is anyway a useful exercise.

Table 1: Starting materials

	SEM02-1	SEM02-6	SEM02-7	SEM02-9	SEM02-11	SEM02-12	SEM02-14	SEM02-15	SEM02-16
SiO$_2$	36·95	49·17	47·69	48·68	49·23	48·65	48·68	48·36	47·69
Al$_2$O$_3$	22·63	20·14	19·54	19·94	20·25	20·80	19·94	19·81	19·54
MgO	35·06	15·35	14·89	15·20	14·75	13·43	15·20	15·10	14·89
CaO	5·36	15·34	14·88	15·19	14·89	14·14	15·19	16·01	14·88
Na$_2$O	0·00	0·00	0·00	0·00	0·00	0·00	1·00	0·00	0·00
H$_2$O	0·00	0·00	3·00	1·00	0·87	2·97	0·00	0·00	0·00
CO$_2$	0·00	0·00	0·00	0·00	0·00	0·00	0·00	0·72	3·00

Table 2: Superliquidus experiments to test starting materials and assembly arrangements

Run no.	SM	AA	T (°C)	t (h)	Thickness (cm)	FTIR no.	H$_2$O (wt %)	CO$_2$ (wt %)
C-1621*	SEM02-6	AA1	1340	24	0·1009	6	0·013(3)†	0·000(0)
C-1809	SEM02-6	AA2	1350	0·33	0·0227	6	0·058(5)	0·000(0)
C-1810	SEM02-11	AA2	1350	0·33	0·0088	6	0·720(12)	0·093(19)
C-1811	SEM02-9	AA2	1350	0·33	0·0080	6	0·858(11)	0·129(25)

SM, starting material; AA, assembly arrangement (see Fig. 1); t, experimental time; FTIR no. is the number of FTIR spectra collected. All uncertainties in this paper are quoted as one standard deviation.
*From Liu & O'Neill (2004*a*).
†0·013(3) is the mean followed by one standard deviation and should be read as 0·013 ± 0·003.

Starting materials

Fine-grained mineral mixes absorb moisture from the atmosphere quite readily. Therefore, because of the desirability of controlling the amounts of H$_2$O loaded into the capsules, glass starting materials were used in this study, rather than pre-crystallized mineral mixes as in our study on the system CMAS–K$_2$O (Liu & O'Neill, 2004*a*). The danger of using glass as the starting material is that it may crystallize initially to minerals with non-equilibrium compositions; for example, to pyroxenes with alumina contents that are too high. Once crystallized, such pyroxenes could fail to re-equilibrate. Here we can check for this problem rigorously, as the equilibrium compositions expected of the pyroxenes are well known (Presnall, 1976; Gasparik, 1984; Sen, 1985; Liu & O'Neill, 2004*a*). Our previous work has shown that pyroxene compositions do change to their equilibrium values on the time scales used in this study, in the presence of melt (Liu & O'Neill, 2004*a*, 2004*b*).

Table 1 lists the compositions of the starting materials. High-purity oxides (SiO$_2$, Al$_2$O$_3$ and MgO), carbonates (CaCO$_3$ and Na$_2$CO$_3$) and hydroxides [Mg(OH)$_2$ and Al(OH)$_3$] were used to prepare these mixtures.

Mixture SEM02-1 was made by melting the decarbonated oxide mix at 1600°C, 1 atm for 15 min. The composition was designed to crystallize to Fo:Sp:Opx: Cpx = 1:1:1:1 (by weight), assuming that Fo and Sp have their pure end-member compositions, whereas Opx and Cpx compositions were from run 116-3 in table 2 of Walter & Presnall (1994).

SEM02-6 is the composition of the isobaric invariant melts for a simplified spinel lherzolite (Sp-lherzolite) in the system CMAS at 1·1 GPa, as obtained from the experimental study in the system CMAS–K$_2$O (Liu & O'Neill, 2004*a*). The glass was prepared at 1400°C, 1 atm, for 20 min before quenching. To produce SEM02-7, SEM02-9, SEM02-11 and SEM02-12, volatile-free glasses with appropriate composition were made first (also 1400°C, 1 atm and 20 min) and then the required amounts of Mg(OH)$_2$ or Al(OH)$_3$, both previously dried at 150°C for 24 h, were added. SEM02-15 was generated by adding ∼1·64% CaCO$_3$ powder, dried at 340°C and stored in a desiccator, to glass SEM02-6. The reason for using hydroxides as the source of H$_2$O was to control the amounts of H$_2$O accurately, given the very low levels of H$_2$O required in our experiments. Unfortunately, these hydroxides may be contaminated with carbonate (see Table 2). To disentangle the effect of CO$_2$ from that of H$_2$O, some experiments were therefore performed with H$_2$O added as distilled H$_2$O. This attempt,
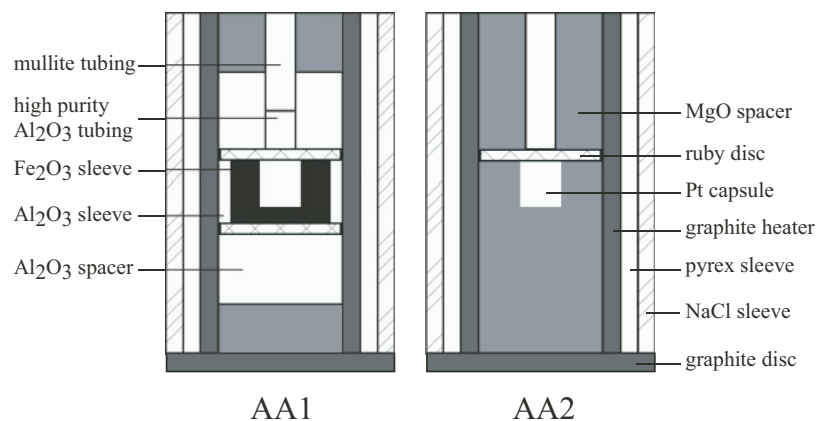
Fig. 1. Experimental assemblies used in this study (not to scale). AA1 with Fe_2O_3 sleeve sample is effective in preventing H_2O and CO_2 from entering the experimental charge, whereas AA2 without the Fe_2O_3 sleeve is open to H_2O, as indicated by our trial experiments (Table 2). For short run times (e.g. 20 min; see run C-1809 in Table 2), AA2 prevents CO_2 entering.

however, was not completely successful either and some CO_2 was still found in the resulting glasses, indicating that the hydroxides were not the only source of carbon contamination. Because the amounts of CO_2 depend approximately on the target amount of H_2O added, H_2O and CO_2 end up being highly correlated in the run products; to circumvent the difficulty that this causes in deconvoluting their effects, we therefore undertook experiments at CO_2-saturated conditions and zero H_2O (it is easier to add an impurity than subtract it). SEM02-16 with 3% CO_2 was made for this purpose by adding $CaCO_3$ to a glass with appropriate composition, which was previously made at 1400°C, 1 bar for 20 min.

To investigate the influence of small amounts of Na_2O in other compositions, apparently present as impurities in the chemicals, glass SEM02-14, with 1 wt % Na_2O, was synthesized at 1400°C and 1 atm for 20 min. All these mixtures were stored in an oven at 150°C during the time this study was carried out.

Experimental procedures

Experiments at 1·1 GPa were made in a conventional 12·7 mm diameter piston-cylinder apparatus (Boyd & England, 1960), using a NaCl–Pyrex assembly, either with or without an Fe_2O_3 sleeve enclosing the capsule (assemblies AA1 and AA2, respectively; Fig. 1). These assemblies have low friction and no pressure correction is thought to be required for the long run times and high temperatures of this study (Green *et al.*, 1966; Bose & Ganguly, 1995; Klemme & O'Neill, 1997). Pt was used as the capsule material. The starting materials were packed into the capsule as layers in the sandwich or half-sandwich geometry. To produce large quench-free melt pools, the relative proportions of the basaltic and the peridotitic materials of the sandwich were adjusted according to the targeted experimental temperatures.

The mass of the charge material in these experiments ranged from 11·6 mg to 19·1 mg, and the ratio of periodotic to basaltic layers ranged from 1:9 to 3:7 approximately. For the hydrous experiments, Pt capsules were welded immediately after loading. Wet tissue was used to blanket the capsule, to prevent any water loss during the welding process (Hibberson, 1978). For nominally anhydrous runs, loaded capsules were stored at 150°C for 6–8 h first and later held in a steel block that had been pre-heated to 750°C while they were welded (Robinson *et al.*, 1998; Liu & O'Neill, 2004*a*).

All experiments were performed using the 'piston-out' method (Johannes *et al.*, 1971). The pressures were continuously monitored and adjusted, if necessary. The continual adjustment of pressure allowed each run to be controlled to within ±0·02 GPa of the nominal pressure. Temperature was measured and controlled with $Pt_{94}Rh_6$–$Pt_{70}Rh_{30}$ (type B) thermocouples; another thermocouple made from the same spools of wire was checked against the melting point of gold at 1 bar, and found to give temperatures within 1°C of the recommended 1064·18°C. Possible pressure effects on the e.m.f. of the thermocouple were ignored. The tip of the thermocouple, the upper ruby disc and at least the uppermost two-thirds of the Pt capsule containing the experimental charge were all carefully placed in the ∼5 mm long hot spot of the experimental assembly. The systematics of the results both in the present study and in closely related previous work (Liu & O'Neill, 2004*a*) are consistent with temperature uncertainties of about ±5°C.

To test various aspects of our experimental protocols, we performed four experiments at superliquidus conditions (Table 2). In none of these experiments could Na_2O be detected by electron microprobe analysis, confirming that the detectable levels found in the melt of most subliquidus experiments are caused by the melt scavenging all the Na_2O impurities in the starting materials.

In anhydrous runs, the assembly arrangement AA1 (with the Fe$_2$O$_3$ sleeve) is effective at keeping out both H$_2$O and CO$_2$, but AA2 (with the MgO sleeve) only keeps out CO$_2$. Unfortunately, both sleeves may permit considerable H$_2$O loss from H$_2$O-rich experimental charges. We were unable to prevent CO$_2$ contamination in any hydrous run. Exactly why C contamination occurs in hydrous runs even when H$_2$O is added directly (i.e. not as hydroxide), but not in anhydrous runs, is not understood.

Analytical conditions—electron microprobe

At the end of a run, the sample was sectioned longitudinally, mounted in epoxy and polished using a series of diamond pastes. Run products were carbon-coated and analysed on a JEOL 6400 scanning electron microprobe in energy dispersive mode (EDS) at the Electron Microprobe Unit (EMU) at ANU. Coexisting phases in all run products were identified by back-scattered electron imaging (Table 3). Beam current was 1 nA, accelerating voltage was 15 keV and analyses were reduced using the ZAF correction procedure (Ware, 1991). A beam spot size of 1 μm was used for all crystalline phases whereas both 1 μm and 10 μm beam spot sizes were used for glass analyses. Analytical accuracy and precision was tested by replicate measurements of two internationally recognized glass standards, GOR132G and KL2G, which have somewhat comparable composition with that of the phases present in this study (Jochum *et al.*, 2000), as reported by Liu & O'Neill (2004*a*).

Besides the expected major component oxides CaO, MgO, Al$_2$O$_3$ and SiO$_2$, all analyses routinely sought Na$_2$O, FeO, Cr$_2$O$_3$ and K$_2$O. The latter three oxides were below the limits of detection and are not considered further, but significant amounts of Na$_2$O were detected in the melt in some runs (up to 1·1 wt %; see Table 4), although it is below the detection limit in the analyses of the glass starting materials, and the test runs designed to check for volatile contents reported in Table 2. To check the accuracy of the Na$_2$O analyses by EDS, several runs were also analysed in wavelength-dispersive mode (WDS) using the Cameca Camebax electron microprobe at the Research School of Earth Sciences, ANU. The higher beam current used in the WDS method reduced the Na$_2$O contents by ∼20%. Because of the good agreement between the EDS analyses and the recommended values of the secondary standards, we believe that the EDS results are more reliable.

Experimental problems and attainment of equilibrium

We identify four potential problems that affect our experiments and seem almost certain to have affected other experimental studies on hydrous partial melting of mantle peridotite:

(1) Pt capsules are open to H because of this component's very rapid diffusion in the temperature regime of interest here. Depending on the details of sample composition and pressure-cell assembly, H$_2$O may increase or decrease during the experiment (and, in Fe-bearing systems, this may be accompanied by oxidation or reduction). Consequently, it is important to analyse H$_2$O after the run, rather than to rely on the amount initially present.

(2) All our experiments with added H$_2$O were contaminated with CO$_2$. This raises the question of whether other studies also suffered this problem, which can be detected only by analysing for CO$_2$ after the run.

(3) The problem of quench-modification of melt compositions becomes increasingly severe with increasing H$_2$O.

(4) The compositions of solid phases with variable composition (here, pyroxenes) need to adjust to their appropriate equilibrium values.

Much of the controversy surrounding apparent discrepancies in experimental results among hydrous partial melting studies have centred on items (3) and (4), but we think that items (1) and (2) present more of an experimental challenge. Item (4), at least, may be evaluated from several lines of evidence, as follows.

(a) The result of previous work in the system CMAS (Presnall *et al.*, 1978; Sen & Presnall, 1984; Liu & Presnall, 1990) suggested that a period of several hours is adequate for the phases observed in this study to establish reversals of phase boundaries at liquidus temperatures. Experiments in the system CMAS + Na$_2$O (Walter & Presnall, 1994) and in the system CMAS + FeO (Gudfinnsson & Presnall, 2000) found that 48 h was long enough for the attainment of equilibrium at temperatures close to the solidi. Most of our experiments were run for longer times.

(b) Duplicate experiments at the relatively low temperatures (for this study) of 1220°C and 1200°C demonstrate that pyroxene compositions are the same after 117 h as after 24 h (Tables 3 and 4).

(c) The solid solutions, Opx and Cpx, in all experiments except the nominally anhydrous experiment C-1812, the experiments close to or below the hydrous solidus (C-1887, C-1859 and C-1858) and a few other assorted cases (C-1878, C-1889, C-1882 and C-1838; see discussion below) show very good homogeneity in composition and demonstrate excellent internal consistency. Their compositions are in excellent agreement with previous work as well (Presnall, 1976; Gasparik, 1984; Sen, 1985; Liu & O'Neill, 2004*a*). The average difference between the calculated temperatures using the geothermometer of Nickel *et al.* (1985) and the nominal experimental

Table 3: Experimental conditions and phase assemblages

Run no.	T (°C)	Time (h)	Starting material	Assembly	Phase observed	$T1$	$T2$	$T3$	$T4$
Experiments in system CMAS + Na$_2$O									
C-1780	1314	70	SEM02-1 + SEM02-14	AA1	Fo + Sp + Opx + Cpx + Melt	1347	1367	1286	1365
C-1773	1310	62	SEM02-1 + SEM02-14	AA1	Fo + Sp + Opx + Cpx + Melt	1339	1359	1273	1369
Experiments in system CMAS + CO$_2$									
C-1812	1317	24	SEM02-1 + SEM02-15	AA1	Fo + Sp + Opx + Cpx + Melt	1340	1385	1273	1375
C-1842	1310	65	SEM02-1 + SEM02-16	AA1	Fo + Sp + Opx + Cpx + Melt + V	1294	1335	1242	1397
C-1885*	1300	48	SEM02-1 + SEM02-16	AA1	Fo + Sp + Opx + Cpx + V An + Opx + Cpx + V				
Experiments in system CMAS + H$_2$O at CO$_2$-rich vapour saturation									
C-1878	1310	66	SEM02-1 + SEM02-16	AA2	Fo + Sp + Opx + (Cpx)† + Melt + V			1246	1407
C-1890	1280	74	SEM02-1 + SEM02-16 + SEM02-9	AA2	Fo + Sp + Opx + Cpx + Melt + V	1257	1301	1246	1383
C-1894	1260	73·5	SEM02-1 + SEM02-16 + SEM02-12	AA2	Fo + Sp + Opx + Cpx + Melt + V	1249	1290	1214	1361
C-1893	1240	73·5	SEM02-1 + SEM02-16 + SEM02-12	AA2	Fo + Sp + Opx + Cpx + Melt + V	1201	1244	1209	1328
Experiments in system CMAS + H$_2$O + CO$_2$ (vapour-unsaturated)									
C-1601	1310	68	SEM02-1 + SEM02-9	AA2	Fo + Sp + Melt				1395
C-1616	1310	49	SEM02-1 + SEM02-9	AA2	Fo + Sp + Opx + Cpx + Melt	1298	1339	1232	1387
C-1750	1310	49	SEM02-1 + SEM02-11	AA2	Fo + Sp + Melt				1411
C-1716	1310	63	SEM02-1 + SEM02-11	AA2	Fo + Sp + Opx + Melt			1223	1405
C-1729	1310	70	SEM02-1 + SEM02-11	AA2	Fo + Sp + Opx + Melt			1214	1403
C-1855	1310	50	SEM02-1 + SEM02-16	AA2	Fo + Sp + Opx + Cpx + Melt	1262	1305	1242	1392
C-1759	1305	49	SEM02-1 + SEM02-6 + SEM02-11	AA2	Fo + Sp + Opx + Cpx + Melt	1320	1364	1255	1393
C-1889	1300	74	SEM02-1 + SEM02-16 + SEM02-9	AA2	Fo + Sp + Opx + (Cpx)† + Melt			1255	1408
C-1602	1300	67	SEM02-1 + SEM02-9	AA2	Fo + Sp + Opx + Cpx + Melt	1281	1325	1242	1381
C-1719	1300	78	SEM02-1 + SEM02-11	AA2	Fo + Sp + Opx + Melt			1232	1404
C-1747	1300	53	SEM02-1 + SEM02-11	AA2	Fo + Sp + Opx + Melt			1228	1387
C-1734	1295	70	SEM02-1 + SEM02-11	AA2	Fo + Sp + Opx + Cpx + Melt	1306	1349	1246	1394
C-1807	1300/1295	24/33	SEM02-1 + SEM02-11	AA2	Fo + Sp + Opx + Cpx + Melt	1324	1363	1251	1386
C-1808	1280/1295	7/15	SEM02-1 + SEM02-11	AA2	Fo + Sp + Opx + Cpx + Melt	1313	1355	1246	1392
C-1611	1280/1290	22/48	SEM02-1 + SEM02-9	AA2	Fo + Sp + Opx + Cpx + Melt	1280	1324	1223	1380
C-1615	1280	75	SEM02-1 + SEM02-9	AA2	Fo + Sp + Opx + Cpx + Melt	1270	1313	1228	1370
C-1723	1290/1280	42·5/48	SEM02-1 + SEM02-11	AA2	Fo + Sp + Opx + Cpx + Melt	1310	1352	1237	1383
C-1724	1270	92	SEM02-1 + SEM02-11	AA2	Fo + Sp + Opx + Cpx + Melt‡	1282	1326	1209	
C-1623	1260	90	SEM02-1 + SEM02-7	AA2	Fo + Sp + Opx + Cpx + Melt	1252	1296	1189	1369
C-1739	1260	88	SEM02-1 + SEM02-12	AA2	Fo + Sp + Opx + Melt			1223	1381
C-1754	1260	94	SEM02-1 + SEM02-12	AA2	Fo + Sp + Opx + Cpx + Melt	1285	1323	1218	1374
C-1881	1260	49·5	SEM02-1 + SEM02-7 + SEM02-15	AA2	Fo + Sp + Opx + Cpx + Melt	1230	1272	1199	1370
C-1882	1260	49·5	SEM02-1 + SEM02-7 + SEM02-15	AA2	Fo + Sp + Opx + (Cpx)† + Melt			1209	1372
C-1622	1240	94	SEM02-1 + SEM02-7	AA2	Fo + Sp + Opx + Cpx + Melt	1219	1262	1204	1362
C-1789	1240	24	SEM02-1 + SEM02-7	AA2	Fo + Sp + Opx + Cpx + Melt	1247	1291	1204	1355
C-1741	1240	95	SEM02-1 + SEM02-12	AA2	Fo + Sp + Opx + Cpx + Melt	1231	1275	1169	1354
C-1633	1220	100	SEM02-1 + SEM02-7	AA2	Fo + Sp + Opx + Cpx + Melt	1200	1243	1164	1355
C-1744	1220	94	SEM02-1 + SEM02-12	AA2	Fo + Sp + Opx + Cpx + Melt	1222	1264	1204	1333
C-1803	1220	24	SEM02-1 + SEM02-12	AA2	Fo + Sp + Opx + Cpx + Melt	1241	1282	1242	1314
C-1636	1200	117	SEM02-1 + SEM02-7	AA2	Fo + Sp + Opx + Cpx + Melt	1183	1224	1143	1335
C-1877	1200	66	SEM02-1 + SEM02-7	AA2	Fo + Sp + Opx + Cpx + Melt	1144	1182	1132	1339
C-1742	1200	117	SEM02-1 + SEM02-12	AA2	Fo + Sp + Opx + Cpx + Melt	1197	1239	1179	1323
C-1817	1335/1200	0·25/65	SEM02-1 + SEM02-6 + H$_2$O	AA2	Fo + Sp + Opx + Cpx + Melt	1232	1275	1169	1353
C-1838	1200	46	SEM02-1 + SEM02-6 + H$_2$O	AA1	Fo + Sp + (Opx)† + Cpx + Melt				1352
C-1886	1180	64·5	SEM02-1 + SEM02-12	AA2	Fo + Sp + Opx + Cpx + Melt‡ An + Sp + Opx + Cpx + Melt	1117	1153	1079	
Experiments in system CMAS + H$_2$O + CO$_2$ at H$_2$O-rich vapour saturation (?)									
C-1887	1160	64·5	SEM02-1 + SEM02-12	AA2	Fo + Sp + Opx + Cpx + Melt‡ + V An + Opx + Cpx + V	1117	1154	1137	
C-1859‡	1150	67·7	SEM02-1 + SEM02-6 + H$_2$O	AA1	Fo + Sp + Opx + Cpx + V An + Opx + Cpx + V				
C-1858‡	1100	67·7	SEM02-1 + SEM02-6 + H$_2$O	AA1	Fo + Sp + Opx + Cpx + V An + Opx + Cpx + V				

AA, assembly arrangement; Fo, forsterite; Sp, spinel; Opx, orthopyroxene; Cpx, clinopyroxene; An, anorthite; V, vapour. Calculated temperatures: $T1$, Nickel *et al.* (1985); $T2$, equation (9) of Brey & Kohler (1990); equation (10) of Brey & Kohler (1990); $T4$, Ford *et al.* (1983).
*Experiments with all phases identified but not quantitatively analyzed because of small sizes of the phases.
†Contains pyroxenes with non-equilibrium compositions (see text); the Al$_2$O$_3$ in these pyroxenes is high and variable, e.g. $15\cdot2 \pm 2\cdot5$ wt % in Cpx in C-1878 (12 analyses).
‡Too small to be accurately analysed.

temperatures is 22 K, further suggesting that Opx and Cpx are in mutual equilibrium.

(d) Good stoichiometry was found for all the solid phases from electron microprobe analysis.

(e) A pair of 'two-stage' reversal experiments (C-1807 and C-1808) have been conducted at 1295°C following the procedure of Presnall *et al.* (1978), Liu & Presnall (1990) and Baker & Stolper (1994). Both the melt compositions and the rim pyroxene compositions from this pair are consistent with each other and with other experiments.

FTIR ANALYSES

It is only relatively recently that analytical methods such as FTIR spectroscopy and SIMS have been applied to experimental studies on mantle melting (Gaetani & Grove, 1998; Falloon *et al.*, 1999, 2001; Falloon & Danyushevsky, 2000; Muntener *et al.*, 2001). Although other methods exist to analyse volatiles in silicate melts, these are unsuitable either for small-scale experiments in which the glass coexists with crystals, or for low volatile contents (King *et al.*, 2002). In this study, the contents of H$_2$O and CO$_2$ in all partial melts were determined by FTIR spectroscopy.

Sample preparation

After analysing all phases by electron microprobe, the samples were prepared as free-standing, doubly polished thin sections for transmission FTIR analysis. The samples were first removed from their epoxy mount and cut using a diamond saw to produce sections with the sample exposed on both the top and bottom surfaces. They were then mounted on glass with crystal-bond and reduced to the desired thickness by manually grinding with a series of silicon carbide abrasive films (3–9 μm) under ethanol or water. Finally both sides were polished using a 1 μm silicon carbide film. The polished sections were removed from the glass base and thoroughly washed in acetone for 30 min to dissolve all the crystal-bond. Each thin section may require 4–10 h of grinding and polishing, depending on the final thickness. The process requires care to prevent the loss of samples during grinding (C-1622 and C-1744 were lost). The sample thicknesses were determined using a micrometer and range from 14 to 490 ± 2 μm (Table 5).

For quantitative FTIR analysis, the thickness of the section has to be tailored to the volatile content of the melt (Ihinger *et al.*, 1994). A number of absorbances may be used for the quantification of water in a silicate glass, each with a different molar absorptivity, resulting in a different optimal sample thickness. For the expected water concentrations the absorbance peak at ∼3550 cm^{-1} is ideal for quantification (of both H$_2$O and OH). This resulted in some thin and difficult-to-

prepare samples; however, the melt pools are not large enough to allow water to be determined from thicker samples using bands at 4500 and 5200 cm^{-1}. CO$_2$ is expected to be present in these glasses exclusively as carbonate (CO$_3^{2-}$), rather than molecular CO$_2$ (Fine & Stolper, 1986; Pan *et al.*, 1991; Pawley *et al.*, 1992; King & Holloway, 2002), which can be quantified from peaks between 1300 and 1700 cm^{-1}. These peaks typically appear as a doublet, with the separation of the components corresponding to the distortion of the CO$_3^{2-}$ group from trigonal planar symmetry. In most cases the H$_2$O and CO$_2$ contents could be determined from samples of a single thickness. Samples were prepared with thicknesses appropriate for the estimated volatile contents determined from the electron microprobe analyses.

FTIR spectroscopy

Transmission IR spectra were recorded using a Bruker A590 IR microscope connected to a Bruker IFS-28 IR spectrometer. The entire system was purged with dry N$_2$ to remove background contributions from atmospheric H$_2$O and CO$_2$. The analysis area was selected using apertures varying between 30 and 100 μm, depending on the size of the crystal-free melt pools. Spectra were recorded from 600 to 5500 cm^{-1} with a resolution of 4 cm^{-1}.

Typical spectra are shown in Fig. 2. The peaks at ∼1520 cm^{-1} and ∼1440 cm^{-1} result from the asymmetric stretch of distorted carbonate groups. The splitting of these peaks is typical of carbonate in basaltic glasses (Fine & Stolper, 1986). The peak at ∼3550 cm^{-1} corresponds to O–H stretching modes of both H$_2$O and OH. The bending mode of H$_2$O occurs at ∼1630 cm^{-1}, which overlaps with the tail of the carbonate bands, which are themselves superimposed on a background derived from silicate bands. The intensity of this tail at 1630 cm^{-1} was determined to be ∼13% of the intensity of the peak at ∼1520 cm^{-1}. Intensity in excess of this amount was observed for samples containing more than ∼2 wt % H$_2$O and indicates the presence of molecular H$_2$O, which may contribute over 30% of the total H content. There is no correlation between the amount of molecular H$_2$O and either total H or C. The weak, broad peak at ∼2400 cm^{-1} derives from water in strongly hydrogen-bonded environments (Zarubin, 1999). There is no evidence of bicarbonate, which would be expected to produce peaks between 2400 and 2620 cm^{-1} corresponding to low-frequency O–H stretching modes (Genge *et al.*, 1995). Molecular CO$_2$, if present, would appear as a single peak at ∼2350 cm^{-1} and is easily distinguished from gaseous CO$_2$ (atmospheric or bubbles), which occurs at a similar energy as a rotational doublet. No absorbance peaks were observed for crystal-bond or

Table 4: Phase composition on a volatile-free basis

Run no.	Phase	CaO	MgO	Al_2O_3	SiO_2	Na_2O*
Experiments in system CMAS + Na₂O						
C-1780, 1314°C	Opx (18)	2·35 (23)†	34·34 (38)	8·89 (46)	54·37 (26)	0·06 (4)
	Cpx (21)	17·97 (42)	21·08 (40)	8·83 (54)	51·90 (38)	0·22 (6)
	Melt (16)	14·67 (18)	13·79 (24)	20·50 (19)	50·01 (16)	1·03 (4)
C-1773, 1310°C	Opx (21)	2·28 (25)	34·21 (36)	9·15 (51)	54·15 (35)	0·22 (6)
	Cpx (21)	18·12 (43)	20·49 (41)	9·17 (50)	51·79 (34)	0·43 (6)
	Melt (15)	13·61 (15)	12·96 (51)	20·92 (50)	50·44 (14)	2·07 (10)
Experiments in system CMAS + CO₂						
C-1812, 1317°C	Opx (16)	2·28 (11)	34·76 (36)	8·52 (60)	54·45 (41)	—
	Cpx (20)	17·79 (78)	21·04 (80)	9·94 (74)	51·23 (67)	—
	Melt (13)	14·91 (31)	14·80 (8)	20·37 (12)	49·52 (13)	0·40 (4)
C-1842, 1310°C	Opx (16)	1·99 (19)	34·66 (32)	8·55 (50)	54·80 (31)	—
	Cpx (17)	18·38 (48)	20·90 (41)	8·63 (60)	52·09 (44)	—
	Melt (13)	14·67 (20)	16·08 (9)	19·96 (13)	49·27 (19)	0·02 (2)
Experiments in system CMAS + H₂O at CO₂-rich vapour saturation						
C-1878, 1310°C	Opx (20)	2·01 (14)	35·15 (27)	8·65 (52)	54·19 (38)	—
	Melt (14)	14·34 (27)	16·59 (16)	19·74 (11)	49·33 (12)	—
C-1890, 1280°C	Opx (18)	2·01 (20)	34·88 (21)	8·50 (31)	54·62 (23)	—
	Cpx (20)	19·14 (21)	20·23 (23)	8·69 (37)	51·95 (28)	—
	Melt (15)	15·37 (13)	15·44 (9)	20·02 (11)	49·16 (17)	—
C-1894, 1260°C	Opx (19)	1·84 (9)	35·29 (30)	8·49 (40)	54·37 (22)	—
	Cpx (21)	19·39 (54)	20·57 (31)	8·14 (45)	51·90 (37)	—
	Melt (15)	15·19 (14)	14·54 (8)	20·64 (10)	49·63 (17)	—
C-1893, 1240°C	Opx (27)	1·82 (18)	35·66 (36)	7·74 (55)	54·75 (31)	—
	Cpx (25)	20·23 (20)	20·02 (39)	7·83 (48)	51·92 (29)	—
	Melt (15)	14·81 (12)	13·18 (11)	21·56 (12)	50·45 (11)	—
Experiments in system CMAS + H₂O + CO₂ (vapour-unsaturated)						
C-1601, 1310°C	Melt (16)	14·02 (14)	15·57 (10)	20·64 (8)	49·25 (14)	0·51 (5)
C-1616, 1310°C	Opx (15)	2·03 (12)	34·81 (16)	8·68 (21)	54·48 (26)	—
	Cpx (17)	19·14 (29)	20·46 (26)	8·59 (25)	51·81 (22)	—
	Melt (16)	14·13 (15)	14·93 (11)	20·50 (14)	49·68 (21)	0·75 (5)
C-1750, 1310°C	Melt (13)	12·68 (15)	16·20 (10)	20·77 (11)	49·72 (13)	0·62 (4)
C-1716, 1310°C	Opx (6)	1·98 (25)	34·45 (35)	9·10 (22)	54·48 (21)	—
	Melt (10)	13·39 (10)	15·84 (18)	20·46 (12)	49·70 (23)	0·62 (5)
C-1729, 1310°C	Opx (20)	1·91 (9)	34·93 (17)	8·48 (32)	54·69 (26)	—
	Melt (12)	13·36 (7)	15·64 (8)	20·55 (9)	49·72 (11)	0·73 (6)
C-1855, 1310°C	Opx (20)	1·99 (16)	34·62 (21)	8·52 (59)	54·87 (35)	—
	Cpx (21)	19·04 (39)	20·27 (37)	8·62 (34)	52·07 (27)	—
	Melt (12)	14·59 (13)	15·87 (12)	20·08 (11)	49·46 (21)	—
C-1759, 1305°C	Opx (16)	2·15 (14)	34·80 (41)	8·25 (52)	54·80 (40)	—
	Cpx (22)	18·47 (33)	20·79 (26)	8·86 (42)	51·88 (31)	—
	Melt (16)	13·96 (17)	15·25 (9)	20·38 (16)	49·73 (19)	0·68 (4)
C-1889, 1300°C	Opx (18)	2·06 (16)	35·08 (22)	8·51 (45)	54·35 (28)	—
	Melt (15)	14·20 (12)	16·65 (10)	19·96 (10)	49·19 (13)	—
C-1602, 1300°C	Opx (28)	2·07 (14)	34·85 (19)	8·56 (27)	54·52 (20)	—
	Cpx (24)	19·49 (23)	20·25 (23)	8·65 (23)	51·61 (18)	—
	Melt (16)	14·89 (12)	14·89 (9)	20·14 (11)	49·58 (14)	0·49 (5)

Run no.	Phase	CaO	MgO	Al₂O₃	SiO₂	Na₂O*
C-1719, 1300°C	Opx (8)	2·04 (11)	34·67 (18)	8·72 (19)	54·58 (16)	—
	Melt (13)	13·59 (16)	15·78 (9)	20·41 (12)	49·58 (15)	0·64 (3)
C-1747, 1300°C	Opx (19)	1·99 (7)	34·65 (10)	8·76 (23)	54·61 (22)	—
	Melt (16)	14·24 (20)	14·95 (16)	20·31 (14)	49·79 (13)	0·72 (4)
C-1734, 1295°C	Opx (17)	2·10 (15)	34·76 (23)	8·38 (44)	54·76 (38)	—
	Cpx (12)	18·88 (43)	20·47 (37)	8·67 (31)	51·97 (21)	—
	Melt (16)	13·82 (14)	15·16 (10)	20·48 (11)	49·77 (13)	0·76 (5)
C-1807, 1295°C‡	Opx (17)	2·14 (12)	34·75 (24)	8·66 (46)	54·45 (29)	—
	Cpx (18)	18·47 (28)	20·84 (32)	8·79 (38)	51·90 (31)	—
	Melt (11)	14·36 (11)	15·12 (9)	20·31 (12)	49·64 (13)	0·57 (5)
C-1808, 1295°C‡	Opx (19)	2·11 (13)	34·90 (25)	8·49 (63)	54·51 (40)	—
	Cpx (19)	18·72 (40)	20·75 (35)	8·65 (41)	51·87 (33)	—
	Melt (17)	14·17 (16)	15·53 (10)	20·33 (11)	49·57 (17)	0·41 (5)
C-1611, 1290°C‡	Opx (21)	1·96 (20)	35·01 (21)	8·49 (38)	54·54 (27)	—
	Cpx (22)	19·49 (28)	20·28 (23)	8·46 (34)	51·77 (23)	—
	Melt (16)	14·94 (19)	14·80 (12)	20·32 (11)	49·40 (19)	0·53 (6)
C-1615, 1280°C	Opx (14)	1·99 (11)	35·13 (24)	8·37 (31)	54·51 (33)	—
	Cpx (22)	19·75 (37)	20·23 (33)	8·30 (32)	51·73 (24)	—
	Melt (16)	15·10 (10)	14·40 (11)	20·39 (12)	49·62 (13)	0·49 (4)
C-1723, 1280°C‡	Opx (17)	2·06 (9)	34·67 (17)	8·58 (38)	54·69 (32)	—
	Cpx (26)	18·80 (34)	20·33 (27)	8·81 (37)	52·06 (24)	—
	Melt (15)	14·02 (17)	14·38 (8)	20·59 (11)	49·90 (13)	1·11 (5)
C-1724, 1270°C	Opx (19)	1·88 (12)	34·89 (15)	8·51 (37)	54·73 (32)	—
	Cpx (25)	19·42 (31)	20·09 (27)	8·59 (41)	51·90 (28)	—
C-1623, 1260°C	Opx (20)	1·78 (19)	35·17 (20)	8·25 (37)	54·80 (24)	—
	Cpx (22)	20·06 (30)	19·90 (31)	8·19 (36)	51·85 (28)	—
	Melt (16)	14·39 (11)	14·30 (13)	20·94 (10)	49·72 (16)	0·64 (7)
C-1739, 1260°C	Opx (20)	1·97 (11)	34·64 (18)	8·94 (32)	54·45 (27)	—
	Melt (14)	14·15 (11)	14·77 (10)	20·69 (15)	49·80 (17)	0·59 (4)
C-1754, 1260°C	Opx (22)	1·95 (13)	34·84 (20)	8·71 (32)	54·51 (23)	—
	Cpx (22)	19·51 (23)	20·30 (35)	7·96 (53)	52·23 (36)	—
	Melt (16)	14·32 (15)	14·36 (7)	20·65 (10)	49·88 (16)	0·79 (5)
C-1881, 1260°C	Opx (20)	1·75 (10)	35·60 (31)	8·18 (59)	54·47 (47)	—
	Cpx (21)	19·74 (34)	20·39 (60)	7·72 (96)	52·14 (51)	—
	Melt (13)	14·80 (16)	14·91 (11)	20·36 (9)	49·93 (13)	—
C-1882, 1260°C	Opx (21)	1·82 (8)	35·23 (21)	8·60 (25)	54·35 (20)	—
	Melt (12)	14·77 (16)	15·00 (9)	20·48 (13)	49·76 (9)	—
C-1622, 1240°C	Opx (16)	1·85 (36)	35·33 (35)	8·07 (35)	54·75 (31)	—
	Cpx (17)	20·74 (45)	19·58 (25)	7·88 (32)	51·80 (20)	—
	Melt (16)	14·86 (14)	13·93 (14)	20·64 (13)	49·81 (20)	0·76 (12)
C-1789, 1240°C	Opx (19)	1·86 (35)	35·08 (45)	8·65 (46)	54·41 (49)	—
	Cpx (23)	20·20 (47)	19·58 (32)	8·49 (59)	51·73 (38)	—
	Melt (12)	14·27 (12)	13·76 (17)	21·33 (10)	50·03 (18)	0·61 (4)
C-1741, 1240°C	Opx (22)	1·67 (9)	35·22 (28)	8·11 (42)	55·00 (25)	—
	Cpx (22)	20·47 (38)	19·60 (40)	7·93 (43)	51·99 (33)	—
	Melt (15)	14·04 (12)	13·53 (12)	21·31 (18)	50·41 (22)	0·71 (5)
C-1633, 1220°C	Opx (15)	1·65 (18)	35·55 (22)	7·90 (19)	54·90 (19)	—
	Cpx (26)	21·03 (25)	19·36 (18)	7·72 (42)	51·89 (31)	—
	Melt (16)	14·49 (16)	13·76 (7)	21·31 (13)	49·84 (16)	0·60 (5)

Table 4: continued

Run no.	Phase	CaO	MgO	Al$_2$O$_3$	SiO$_2$	Na$_2$O*
C-1744, 1220°C	Opx (22)	1·86 (21)	34·99 (30)	8·47 (43)	54·68 (27)	—
	Cpx (22)	20·73 (17)	19·35 (27)	8·06 (49)	51·87 (32)	—
	Melt (16)	14·39 (14)	12·82 (9)	21·67 (5)	50·54 (14)	0·58 (6)
C-1803, 1220°C	Opx (22)	2·09 (24)	34·89 (27)	8·51 (63)	54·51 (41)	—
	Cpx (19)	20·42 (35)	18·56 (44)	8·07 (60)	51·96 (33)	—
	Melt (13)	13·91 (14)	12·04 (8)	22·38 (8)	51·06 (19)	0·61 (5)
C-1636, 1200°C	Opx (16)	1·53 (6)	35·65 (12)	7·88 (17)	54·94 (19)	—
	Cpx (18)	21·31 (37)	19·22 (34)	7·64 (34)	51·83 (26)	—
	Melt (15)	14·62 (11)	13·08 (10)	21·68 (12)	50·18 (18)	0·45 (6)
C-1877, 1200°C	Opx (20)	1·41 (10)	35·92 (16)	7·99 (34)	54·68 (28)	—
	Cpx (21)	21·06 (31)	19·45 (27)	7·49 (54)	51·99 (39)	—
	Melt (13)	14·82 (22)	13·62 (10)	21·40 (10)	50·16 (14)	—
C-1742, 1200°C	Opx (26)	1·73 (24)	35·20 (36)	8·22 (41)	54·85 (30)	—
	Cpx (26)	21·12 (22)	19·16 (31)	7·87 (65)	51·85 (40)	—
	Melt (14)	14·27 (18)	12·50 (9)	21·88 (12)	50·81 (18)	0·54 (4)
C-1817, 1200°C‡	Opx (22)	1·67 (11)	35·55 (23)	8·07 (47)	54·71 (28)	—
	Cpx (22)	20·46 (41)	19·73 (38)	7·88 (71)	51·93 (46)	—
	Melt (14)	14·26 (14)	13·90 (9)	21·56 (12)	49·87 (13)	0·41 (4)
C-1838, 1200°C	Cpx (19)	20·71 (41)	19·12 (46)	8·02 (53)	52·16 (41)	—
	Melt (10)	14·05 (11)	12·34 (11)	22·02 (7)	51·34 (14)	0·26 (5)
C-1886, 1180°C	Opx (20)	1·19 (7)	36·33 (25)	7·43 (33)	55·05 (34)	—
	Cpx (19)	21·41 (37)	19·39 (20)	7·25 (78)	51·95 (47)	—
	Opx (17)	1·48 (17)	35·66 (28)	8·46 (26)	54·39 (19)	—
	Cpx (19)	21·65 (32)	18·88 (25)	7·50 (49)	51·96 (42)	—
	An (11)	19·77 (20)	0·26 (8)	36·49 (37)	43·49 (36)	—
	Melt (12)	13·78 (12)	10·84 (14)	22·93 (10)	52·29 (23)	0·16 (4)
Experiments in system CMAS + H$_2$O + CO$_2$ at H$_2$O-rich vapour saturation (?)						
C-1887, 1160°C	Opx (23)	1·44 (11)	36·11 (31)	7·64 (90)	54·81 (61)	—
	Cpx (22)	21·38 (30)	19·25 (43)	7·70 (69)	51·67 (45)	—
	Opx (21)	1·52 (19)	35·88 (47)	7·53 (61)	55·06 (32)	—
	Cpx (22)	21·14 (42)	19·51 (39)	6·85 (65)	52·51 (52)	—
	An (18)	19·54 (18)	0·31 (10)	36·17 (28)	43·80 (34)	0·18 (7)

*Na$_2$O content reported for melts in all experiments was given by EDS whereas that for Opx and Cpx in C-1780 and C-1773 is by WDS.
†Average followed by one standard deviation, read as 2·35 ± 0·23.
‡Final experimental temperature from 'two-stage' experiments.

epoxy, which have intense bands in the C–H stretching region ($\sim$2900 cm^{-1}).

The spectra of all samples exhibit the H$_2$O/OH and CO$_3^{2-}$ bands shown in Fig. 2, which are characteristic of silicate glasses. In addition, sample C-1616, uniquely contains a sharp peak $\sim$1700 cm^{-1}, which energy is typical of a carbonyl stretching mode, although the nature of the structural unit and the reason for its occurrence in this sample is unclear.

The H$_2$O and CO$_2$ contents of the samples were determined from the absorbance above background of the corresponding bands. The background was modelled by a straight line through the minima at the high and low wavenumber ends of the absorption peaks. The absorbance values are given in Table 5.

Quantifying H$_2$O and CO$_2$ in melts

The volatile content of each sample was determined using the relationship

$$c = \frac{M_w A}{d\rho\varepsilon} \times 100 \qquad (1)$$

Table 5: FTIR data

Run no.	d (cm)	ρ (g/l)	No. of spectra	H_2O		CO_2	
				Absorbance	H_2O (wt %)	Absorbance	CO_2 (wt %)
Experiments in system CMAS + CO_2							
C-1812	0·0091	2776	6	0·050(6)*	0·05(1)	1·213(74)	0·56(7)
C-1842	0·0490	2789	8	0·733(12)	0·14(1)		
	0·0071	2789	18			1·041(20)	0·62(3)
Experiments in system CMAS + H_2O at CO_2-rich vapour saturation							
C-1878	0·0059	2779	8	0·224(7)	0·37(2)	0·917(19)	0·66(4)
C-1890	0·0062	2770	5	0·378(6)	0·59(3)	1·027(26)	0·70(4)
C-1894	0·0034	2732	7	0·377(12)	1·19(8)	0·576(27)	0·73(6)
C-1893	0·0049	2682	7	0·798(7)	1·63(8)	0·864(15)	0·77(4)
Experiments in system CMAS + H_2O + CO_2 (vapour-unsaturated)							
C-1601	0·0136	2748	5	0·843(11)	0·61(7)	0·418(22)	0·13(2)
C-1616	0·0169	2754	4	0·685(4)	0·40(4)	0·478(16)	0·12(1)
C-1750	0·0103	2751	3	0·490(8)	0·46(5)	0·300(9)	0·12(1)
C-1716	0·0223	2763	4	0·638(21)	0·28(3)	0·373(52)	0·07(1)
C-1729	0·0124	2764	7	0·259(3)	0·20(2)	0·156(7)	0·05(1)
C-1855	0·0172	2750	6	0·390(22)	0·72(5)	0·796(33)	0·64(4)
C-1759	0·0222	2766	6	0·472(11)	0·21(2)	0·187(24)	0·04(1)
C-1889	0·0069	2778	7	0·315(9)	0·44(2)	0·955(24)	0·58(3)
C-1602	0·0152	2734	3	0·955(5)	0·62(7)	0·636(22)	0·18(2)
C-1719	0·0158	2764	6	0·556(12)	0·34(4)	0·382(21)	0·10(1)
C-1747	0·0192	2763	3	0·493(19)	0·25(3)	0·085(6)	0·02(0)
C-1734	0·0164	2758	6	0·581(15)	0·35(4)	0·443(19)	0·11(1)
C-1807	0·0079	2765	5	0·248(5)	0·30(4)	0·451(14)	0·24(3)
C-1808	0·0054	2769	5	0·178(10)	0·33(4)	0·112(11)	0·09(1)
C-1611	0·0070	2734	4	0·633(7)	0·89(10)	0·579(15)	0·35(4)
C-1615	0·0068	2729	3	0·654(14)	0·95(11)	0·542(19)	0·34(4)
C-1723	0·0060	2718	6	0·546(6)	0·90(11)	0·696(7)	0·50(6)
C-1623	0·0067	2703	4	0·900(47)	1·33(17)	0·589(26)	0·38(5)
C-1739	0·0087	2725	5	0·937(40)	1·06(13)	0·543(17)	0·27(3)
C-1754	0·0080	2726	7	0·767(30)	0·94(11)	0·548(20)	0·29(4)
C-1881	0·0073	2707	5	1·122(7)	1·53(6)	0·815(16)	0·48(2)
C-1882	0·0048	2730	8	0·561(26)	1·15(8)	0·415(12)	0·37(2)
C-1789	0·0047	2630	5	1·199(125)	2·31(41)	0·490(8)	0·47(9)
C-1741	0·0058	2666	10	1·062(64)	1·85(24)	0·476(38)	0·36(5)
C-1633	0·0065	2619	5	1·914(20)	2·98(35)	1·157(30)	0·80(9)
C-1803	0·0037	2623	1	0·831	2·30	0·228(5)	0·28(3)
C-1636	0·0014	2555	8	0·552(31)	4·16(79)	0·216(15)	0·71(14)
C-1877	0·0047	2600	5	1·590(41)	3·50(20)	0·853(32)	0·82(5)
C-1742	0·0025	2626	8	0·623(35)	2·55(38)	0·225(17)	0·40(6)
C-1817	0·0024	2643	7	0·630(41)	2·67(41)	0·350(25)	0·65(10)
C-1838	0·0048	2623	7	1·173(45)	2·50(16)	0·202(11)	0·19(1)
C-1886	0·0039	2575	6	1·145(26)	3·07(20)	0·245(16)	0·29(3)

*Average followed by one standard deviation, read as 0.050 ± 0.006.
The one standard deviation of H_2O and CO_2 is given by

$$\sigma(c)^2 = \left(\frac{M_w A}{d\rho\varepsilon}\right)^2 \left[\frac{\sigma(A)^2}{A^2} + \frac{\sigma(d)^2}{d^2} + \frac{\sigma(\rho)^2}{\rho^2} + \frac{\sigma(\varepsilon)^2}{\varepsilon^2}\right].$$

We assumed uncertainties (one standard deviation) of 2 µm for the thickness measurement (d), 5% for the calculated density (ρ) and 10% for the calibration factor (ε). Thicknesses calculated from interference fringes are: C-1723, 61·7 µm; C-1742, 28·2 µm; C-1636, 18·7 µm. (See text for details.)

where c is the concentration of H_2O or CO_2 in wt %, M_w is the molecular weight of H_2O (18·02) or CO_2 (44·01), A is the absorbance, d is the thickness of the sample (cm), ρ is the density of the melt (g/l), and ε the extinction coefficient (L/mol per cm) for H_2O [67 from Stolper (1982b) for the band at 3550 cm^{-1}] or for CO_2 [375 from Fine & Stolper (1986) for the band at $\sim$1520 cm^{-1}]. The calculated H_2O and CO_2 contents are given in Table 5. The uncertainty in thickness dominates the relative uncertainty for the thinnest sections, which correspond to the highest H_2O contents. Unusually for an analytical procedure this
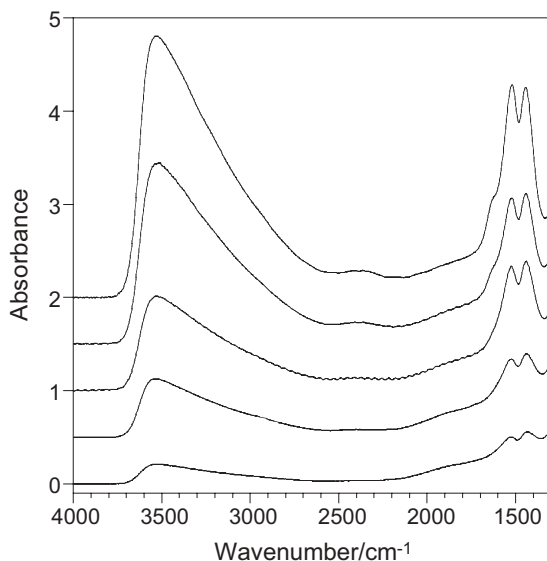
Fig. 2. Infrared absorption spectra of glasses in samples (from bottom to top) c1729, c1601, c1754, c1741, and c1817, showing a concomitant increase in CO_2 (dissolved as CO_3^{2-}, doublet $\sim$1500 cm^{-1}) with increasing H_2O (dissolved as both OH$^-$ and H_2O, broad band $\sim$3550 cm^{-1}). The shoulder on the high-energy side of the CO_3^{2-} bands at high H_2O contents corresponds to molecular H_2O. The spectrum for sample c1754 exhibits oscillations (particularly $\sim$2500 cm^{-1}) called interference fringes. The spectra are normalized to a sample thickness of 100 μm and offset for clarity.

method returns lower precision the higher the amount analysed.

The density, ρ, of each sample was determined using the program Magma2 (Wohletz, 1996). Available density–composition data in the literature were used to check the program. It was found that Magma2 accurately reproduces the density of low-FeO glasses regardless of the pressure and temperature at which they were produced. The calculation was done iteratively starting from an initial guess for the density, and CO_2 was ignored. The calculated densities are listed in Table 5. The uncertainty in the density calculation is estimated to be <3%. The relative difference between the maximum density (2789 g/l, C-1812) and the minimum density (2555 g/l, C-1636) is less than 10%, so that the assumption of constant density used in the previous studies of Stolper & Holloway (1988), Pan *et al.* (1991) and Pawley *et al.* (1992) is reasonable.

The spectra of some thin, parallel, sections contain interference fringes, which can be used to determine the sample thickness from

$$d = 1/(2n\upsilon) \qquad (2)$$

where *d* is the thickness (cm), *n* is the refractive index of the glass, and υ the wavelength (cm^{-1}) of the fringes. The refractive index was estimated by the method of Church & Johnson (1980), which ignores H_2O and CO_2. The

calculated thicknesses are slightly larger than the measured values and the differences (1·7 μm for C-1723, 3·2 μm for C-1742, and 4·7 μm for C-1636) are positively correlated with the missing mass in the refractive index calculation. Taking this into account, the calculated values are in reasonable agreement with the direct measurements, justifying our estimation of an uncertainty of ±2 μm.

EXPERIMENTAL RESULTS

Table 3 summarizes the starting materials, the piston-cylinder pressure assemblies used, the run conditions and the phases observed in our 47 experiments. The temperature range covered in this study is from 1100 to 1317°C, with run durations from 24 to 117 h; most runs were longer than 48 h. Although a number of other phase assemblages were observed in this study, we focus here on the experiments that produced our target multiply saturated assemblage Fo + Sp + Opx + Cpx + Melt ± Vap.

The compositions of Opx, Cpx and Melt from electron microprobe analyses, normalized to 100%, are presented in Table 4. Melt compositions are given on a volatile-free basis. Volatile contents from FTIR spectroscopy are given in Table 5.

Compositions of crystalline phases

In this study, Fo, Sp and An have almost pure end-member compositions, although Fo has $\sim$0·3 wt % CaO, generally consistent with the amounts expected from previous work (e.g. Köhler & Brey, 1990; Libourel, 1999; Liu & O'Neill, 2004*a*, 2004*b*).

Three types of pyroxenes were observed in this study: equilibrium pyroxenes, quench pyroxenes, and high-Al disequilibrium pyroxenes. Quench pyroxenes (mostly Cpx) were feathery, small (<2 μm across) and often apparently non-stoichiometric with high but variable Al_2O_3 content. They are present in almost all melt-bearing experiments mainly as overgrowths on other solid phases (mostly Opx). The high-Al disequilibrium pyroxenes were observed as free-standing crystals (not attached to any other solid phases) in C-1878 (Cpx), C-1889 (Cpx), C-1882 (Cpx), and C-1838 (Opx). Although these pyroxenes were euhedral, stoichiometric and of 5–10 μm size, their Al_2O_3 contents are anomalously high when compared either with the trend established by Cpx and Opx in other experiments (which are consistent with previous studies), or with the 'equilibrium' pyroxene in the same experiments (only the latter are given in Table 4). Their Al_2O_3 is also variable. We believe that these pyroxenes crystallize from the melts towards the end of the experiments, giving them insufficient time to re-equilibrate with the other phases. The reason for their appearance would be

because the initial H_2O in C-1878, C-1889, C-1882 and C-1838 was too high at the temperature of the experiments for saturation in Cpx (or Opx in C-1838), but loss of H_2O during the experiment by diffusion of H_2 through the Pt capsule brings on saturation. These runs have not been used in determining the multiply saturated melt compositions as a function of volatile contents, nor have the anomalous pyroxene compositions been included in the discussion below.

The equilibrium pyroxenes in our experiments are very homogeneous and generally contain negligible amounts of Na_2O, except for Cpx in the runs where Na_2O was deliberately added. The geothermometer of Nickel *et al.* (1985) using the exchange of Ca between Opx and Cpx and calibrated from their experiments in the system CMAS reproduces our nominal experimental temperatures very well, with an average difference of 22 degrees (Fig. 3). This agreement implies excellent consistency between our results and the experiments of Nickel *et al.* (1985). Of other two-pyroxene geothermometers, equation (9) of Brey & Köhler (1990) gives systematically higher and more scattering of calculated temperatures with an average difference of 40 degrees, whereas equation (10) of Brey & Köhler (1990) gives systematically lower calculated temperatures, with an average difference of 53 degrees. These results are similar to that found in our previous study of the system CMAS–K_2O (Liu & O'Neill, 2004*a*).

Phase relationships with small amounts of volatiles (H_2O and CO_2)

Figure 4 summarizes the contents of H_2O and CO_2 in our multiply saturated melts (the assemblage Fo + Sp + Opx + Cpx + Melt). This assemblage is isobarically invariant in the volatile-free CMAS system, and exists at 1320 ± 10°C at 1·1 GPa (Liu & O'Neill, 2004*a*). The addition of H_2O introduces one degree of freedom (at 1·1 GPa), such that the temperature at which the assemblage exists is lowered according to the H_2O content of the melt. Here we have to acknowledge that although our experiments were designed to study the effect of H_2O, we were unable to produce H_2O-containing melt that did not also contain CO_2, hence a discussion of the relevant phase relations in CMAS–H_2O based directly on our results without some modelling is not possible. Rather, we must deconvolute the effects of H_2O from those of CO_2 and indeed Na_2O, but first we provide a brief description of the experimental results without such manipulation.

The lowest temperature at which we unambiguously observed melt was 1180°C (C-1886); however, the two parts of the sandwich in this experiment are not in equilibrium. The original melt 'filling' has produced Sp + Opx + Cpx + An + Melt, whereas the sandwiching layers retain Fo + Sp + Opx + Cpx + Melt. However, the compositions of Opx and Cpx in the different layers are very similar, suggesting that this run is close to the isobaric invariant point in the five-component CMAS–H_2O system Fo+ Sp + Opx + Cpx + An + Melt, which occurs where the reaction Fo + An = Opx + Cpx + Sp intersects the solidus. The three experiments at lower temperatures (C-1887, C-1859 and C-1858) unfortunately produced ambiguous results. In all three, the 'filling' and the 'sandwiching' layers are not in equilibrium. A small amount of melt was observed at 1160°C (C-1887) in the Fo + Opx + Cpx + Sp 'sandwiching' layers, but the 'filling' had completely crystallized to An + Opx + Cpx. The experiments at 1150°C and 1100°C were melt-free; however, it is not clear what the composition of the vapour in these experiments was (i.e. H_2O/CO_2 ratio). Usually H_2O is used to enhance reaction rates and to grow large crystals in high-pressure experiments, yet the run products in these experiments were too small to analyse. Only <4 wt % H_2O was added in these experiments, which is too little to be detected by weight loss after a run. At 1·0 GPa, Yoder (1971) reported the phase assemblage Fo + Sp + Opx + Melt + Vap down to ~1000°C and Sp + Opx + Cpx + Melt + Vap to ~900°C in the system Di–Pyrope–H_2O; it is likely that his experiments were of much shorter duration (judging by analogous experiments carried out in the Geophysical Laboratory in that era), which may have minimized CO_2 contamination, if this occurs by diffusion through the Pt capsule. Hence the failure to observe melt in our low-temperature runs may be due to such contamination.

Although we could not achieve H_2O-containing melt without CO_2, we could produce almost H_2O-free experiments with CO_2 (Fig. 4). Adding CO_2 to the system CMAS lowers the partial melting temperature very slightly; the isobarically invariant phase assemblage Fo + Sp + Opx + Cpx + Melt + CO_2-Vap is observed at 1310 ± 5°C, and the CO_2 solubility in the melt is 0·62 wt %. The difference between this solidus and the vapour-absent solidus is at the resolution of our experiments in terms of temperature measurement, and another run at 1300°C (C-1885) is subsolidus. It is worth pointing out here that the CO_2-vapour is very inefficient in transporting material, so that all the solid phases in C-1885 were small and their compositions were variable and not in equilibrium.

When both H_2O and CO_2 are added to the system CMAS, the stable phase assemblage Fo + Sp + Opx + Cpx + Melt becomes isobarically divariant, whereas the phase assemblage Fo + Sp + Opx + Cpx + Melt + Vap is isobarically univariant. This latter curve is well determined (five experiments at 1310–1240°C) and is plotted in Fig. 4. Remarkably, the curve has a positive slope in this part of the diagram, that is, the solubility of CO_2
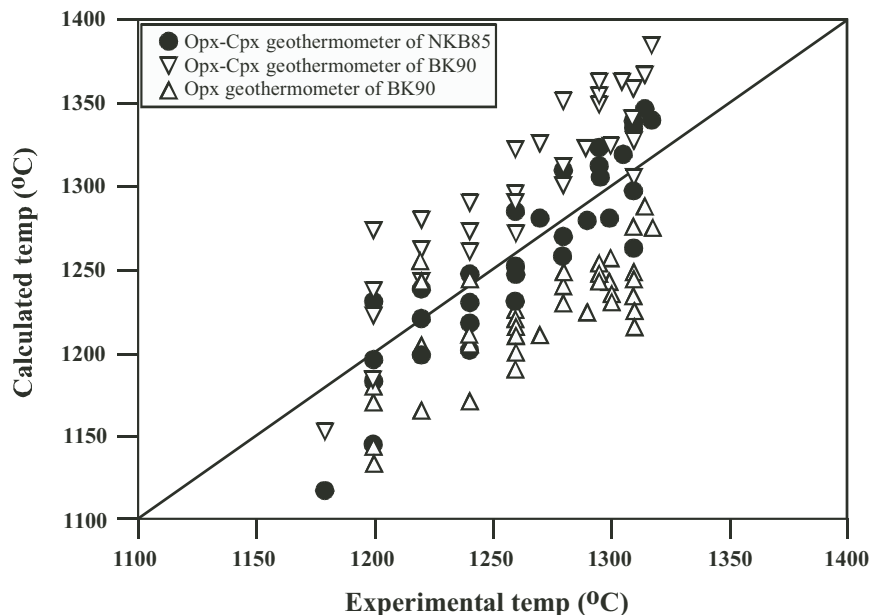
Fig. 3. A comparison diagram of experimental vs calculated temperatures using two-pyroxene geothermometery. NKB85, Nickel *et al.* (1985); BK90, Brey & Köhler (1990), their equations (9) and (10). (See Table 3 for the pyroxene compositional data.) To display the data more clearly, some points have been plotted slightly shifted horizontally.

increases with H_2O, despite the fact that the partial pressure of CO_2 (pCO_2) at vapour saturation obviously must decrease as H_2O is added to the system. Thus the increasing solubility of CO_2 with H_2O must be due to a strong 'interaction' between CO_2 and H_2O in silicate melts, although there is no evidence for a directly combined species such as bicarbonate (HCO_3^-) in the FTIR spectra. [For an example of a diagram showing what would theoretically be expected without such strong CO_2–H_2O interactions, albeit at much lower pressure, see Stolper & Newman (1994, fig. 1).] It appears that the decrease of pCO_2 is small because the partition coefficient of H_2O between Melt and Vap is much greater than that of CO_2, and therefore the decrease is more than counterbalanced by the chemical effect that H_2O in the melt has on enhancing CO_2 solubility (Mysen, 1976)—it should be noted that H_2O depolymerizes the melt, making it more basic, and basic melts have higher CO_2 solubility than polymerized, acidic melts. Exactly the same phenomenon was found by King & Holloway (2002) in andesitic melts, and has also been reported in dacitic melts by Behrens *et al.* (2004).

Compositions of melts

Although quench Cpx, present as overgrowths, usually 1–2 μm thick, mainly rimming pre-existing stable Cpx and Opx, was observed in all melt-bearing experiments, because of the sandwich geometry used in this study, pockets of melt with a diameter >100 μm were observed

in all experiments except C-1724 and C-1773. Such pockets are sufficiently large that mass-balance calculations show that their middle portions are unaffected by this quench modification. The extent of partial melting in C-1724 is very low and a good analysis of the melt was not possible. The melt in C-1773 was analysed and the result appears consistent with that from other experiments, although observed standard deviations are larger. All other experiments produce homogeneous melt, with typical standard deviations (in wt %) ranging from ±0·04% for Na_2O to ±0·20% for SiO_2.

The compositions of melts are plotted in Fig. 5, in the projections from Diopside [Di: $CaMgSi_2O_6$] onto the plane JdCaTsLc–Ol–Qz (Jd = $NaAlSi_2O_6$, CaTs = $CaAl_2SiO_6$, Lc = $KAlSi_2O_6$; Fig. 5a)], from olivine onto the plane JdCaTsLc–Di–Qz (Fig. 5b) and from AbAnOr (Ab = $NaAlSi_3O_8$; An = $CaAl_2Si_2O_8$; Or = $KAlSi_3O_8$) onto the plane Ol–Di–Qz (Fig. 5c; Falloon & Green, 1988). The melt at the invariant point Fo + Sp + Opx + Cpx + Melt in the system CMAS at 1·1 GPa is an olivine tholeiite (Fig. 5b). The effect of Na_2O is to shift the composition towards the silica-undersaturated plane Di–Fo whereas the effect of H_2O moves the melt composition in the opposite direction in this projection, towards the plane AbAnOr–En (En = $Mg_2Si_2O_6$), the melts becoming quartz-normative at ~3% H_2O. Figure 5a and c shows that the Di component of the melt is substantially depressed by H_2O. It should be noted that we have not attempted any correction in the plotted data in this figure for the small amounts of Na_2O and CO_2 present. Any
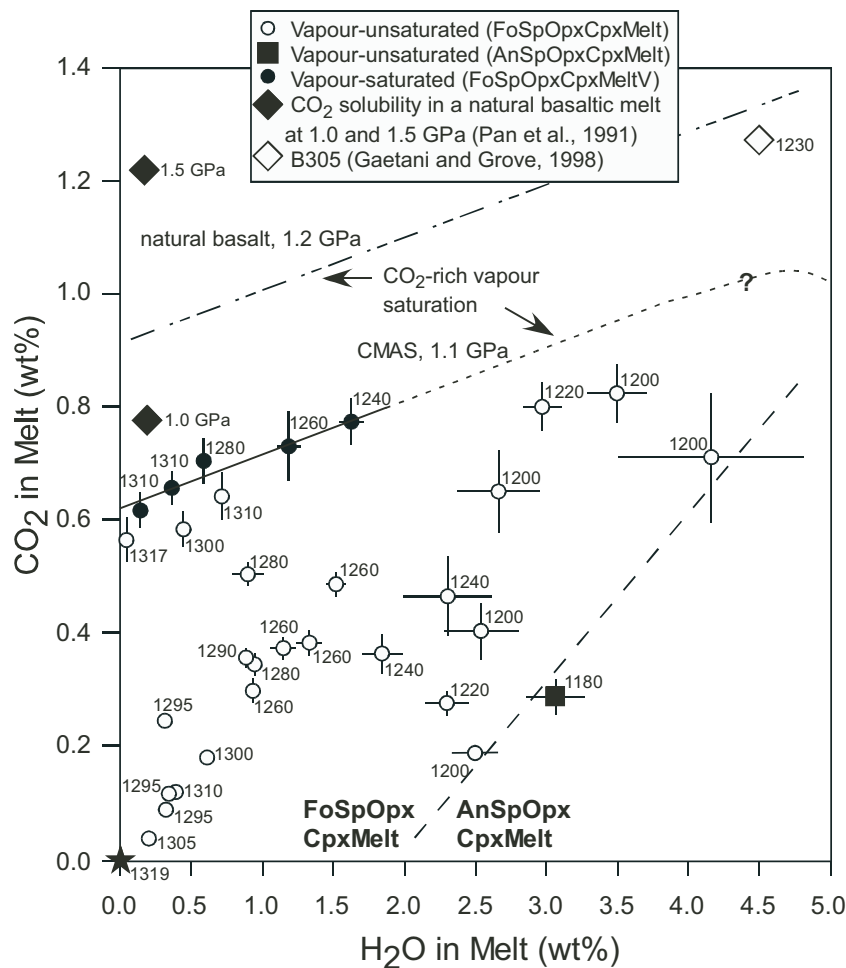
Fig. 4. Multiply saturated (Fo + Sp + Opx + Cpx + Melt ± Vap) melting in the system CMAS ± H$_2$O ± CO$_2$ at 1·1 GPa: a summary of the H$_2$O and CO$_2$ contents in the experimentally produced melts. Numbers alongside the symbols are experimental temperatures in °C. The solidus temperature in CMAS (1319°C) is from Liu & O'Neill (2004*a*), plotted as the filled star. Most data are vapour-unsaturated, but five data on melts saturated with CO$_2$-rich vapour define a straight line with positive slope in this diagram. It should be noted that this vapour-saturation line must bend round to intersect the H$_2$O axis, albeit metastably because of hydrous solid phases replacing the Fo + Sp + Opx + Cpx assemblage. Also plotted are the solubilities of CO$_2$ in a natural basaltic melt at 1·0 GPa and 1300–1500°C (0·77 ± 0·07 wt %) and 1·5 GPa and 1400–1600°C (1·21 ± 0·13 wt %) at ~0·2 wt % H$_2$O, from Pan *et al.* (1991). For CO$_2$-rich vapour saturation in natural basaltic melts at 1·2 GPa, we infer a straight line with a slope similar to that in CMAS, to join the results of Pan *et al.* (1991) at very low H$_2$O with the experimental datum B305 of Gaetani & Grove (1998), thus implying consistency between these two studies, if the effect of H$_2$O on CO$_2$ solubility in natural systems is the same as we find in CMAS. The transition from the Sp-lherzolite assemblage to the Anorthite (An)-bearing assemblage as a result of the reaction Opx + Cpx + Sp = Fo + An (see Liu & O'Neill, 2004*a*), which our (unreversed) results locate between 1180 and 1200°C, is indicated by a dashed line.

effects of CO$_2$ on the melt composition are too small to be noticeable in our H$_2$O-poor experiments. This is not surprising given the low solubility of CO$_2$ in the silicate melts at 1·1 GPa (0·62 wt %).

The effect of Na$_2$O: partial melting in system CMAS–Na$_2$O

The trace amount of Na$_2$O apparently present in the starting materials has been concentrated into the melt, reaching levels as high as ~1·1 wt % (Table 4). This is too high an amount to ignore in the present context, and it is

necessary to assess what effects Na$_2$O has on the partial melting process, so that an appropriate correction may be applied. Accordingly, two experiments were performed adding small amounts of Na$_2$O under anhydrous conditions, using the sandwich technique as in our previous work on the system CMAS + K$_2$O (Liu & O'Neill, 2004*a*). A much more extensive study of partial melting in CMAS + Na$_2$O has been undertaken by Walter & Presnall (1994), from 0·7 to 3·5 GPa.

The results of Walter & Presnall (1994), as parameterized by them in the form of equations describing the effect of Na$_2$O on temperature and melt composition,
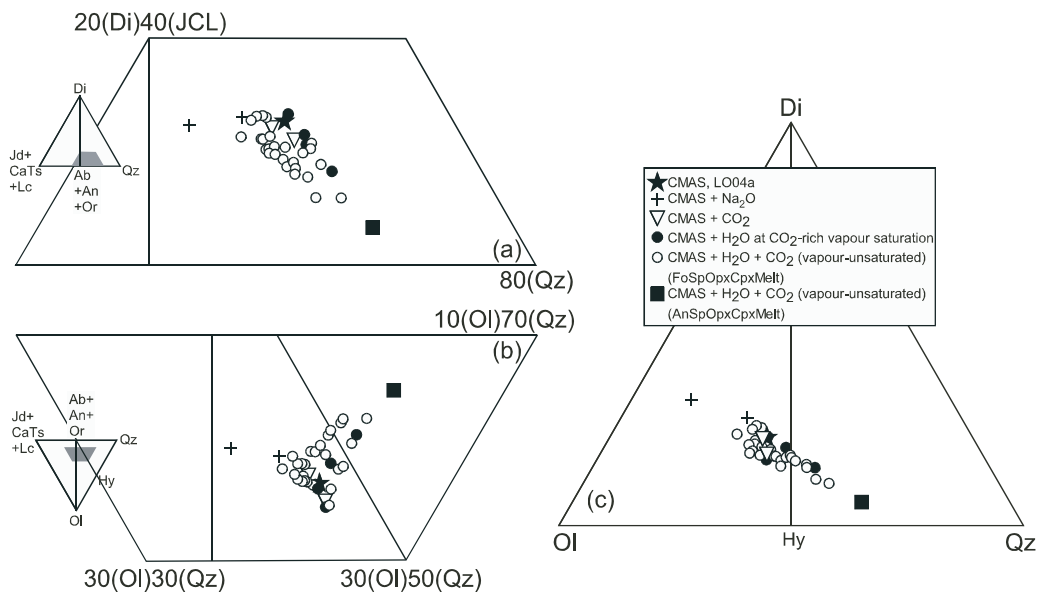
Fig. 5. Experimentally produced melts plotted onto: (a) the plane JdCaTsLc–Di–Qz from Ol; (b) the plane JdCaTsLc–Ol–Qz from Di; (c) the plane Ol–Di–Qz from AbAnOr. Plotting procedures have been described by Falloon & Green (1988). The isobarically invariant melt composition for the Sp-lherzolite in the system CMAS at 1·1 GPa is from Liu & O'Neill (2004a) (LO04a).

are compared with our data at 1·1 GPa in Fig. 6. It may be seen that there is good agreement as regards the compositional effects, but the parameterization of Walter & Presnall (1994) appears to show a substantially greater decrease in solidus temperature. This may be an experimental artefact caused by the solidus temperature of Walter & Presnall (1994) for the pure CMAS system being too high, which we have argued previously from independent evidence (Liu & O'Neill, 2004a). The reason is as follows. The solidus temperature in CMAS of Walter & Presnall (1994) is constrained at 1·1 GPa by experiment 116-3 from the earlier work of Presnall *et al.* (1979). This earlier work used W–Re thermocouples, which (amongst their other problems) may oxidize in the piston-cylinder apparatus at relatively low pressures, as the alumina thermocouple tubing does not collapse completely unless pressures are greater than ∼1·0–1·5 GPa; this allows oxygen from the air to leak in and attack the hot end of the thermocouple (e.g. Falloon *et al.*, 2001). Oxidation causes drift to higher apparent temperatures. Walter & Presnall (1994) guarded against this oxidation by flowing N_2 around the thermocouple, but this was not done in the earlier work. It is possible, therefore, that there is a systematic offset in temperature measurement between the new experiments in CMAS + Na_2O reported by Walter & Presnall (1994), which appear to be consistent with our work, and the older experiments in the pure CMAS system from Presnall *et al.* (1979) below about 1·5 GPa. When the two sets of experiments are spliced together, this offset results in an artificially large effect of small amounts of Na_2O on the solidus temperature. Here we

find that the effect of Na_2O in depressing the solidus at 1·1 GPa is ∼4°C/wt % Na_2O (Fig. 6a), as compared with ∼10°C/wt % Na_2O claimed by Walter & Presnall (1994). Wasylenki *et al.* (2003) have recently reported that Na_2O depresses the solidus of natural peridotite by ∼4°C/wt % Na_2O, in agreement with our results. The effect of K_2O on the solidus reported by Wasylenki *et al.* (2003) was ∼7°C/wt % K_2O, which is also in excellent agreement with the result of our recent study (∼6°C/wt % K_2O; Liu & O'Neill, 2004a).

It is a startling observation that the effect of Na_2O on the multiply saturated melt composition at 1·1 GPa is profoundly different from that of K_2O (Liu & O'Neill, 2004a), producing almost opposite trends on most projections. Whereas increasing Na_2O drives melt compositions towards nepheline-normative conditions, increasing K_2O moves the compositions towards the quartz-normative field. Yet Na_2O and K_2O are often lumped together in igneous petrology, particularly in rock classification schemes, as in AFM diagrams or the 'alkali index' (e.g. Wilson, 1989, pp. 8–10).

Effect of H_2O on the partial melting temperature and melt composition of spinel lherzolite in CMAS–H_2O at 1·1 GPa

Having admitted failure in our efforts to produce experiments not contaminated by Na_2O and CO_2, we had then planned to determine the effects of Na_2O and CO_2 on the multiply saturated melting in CMAS in the H_2O-free systems, as discussed in the previous sections, so that
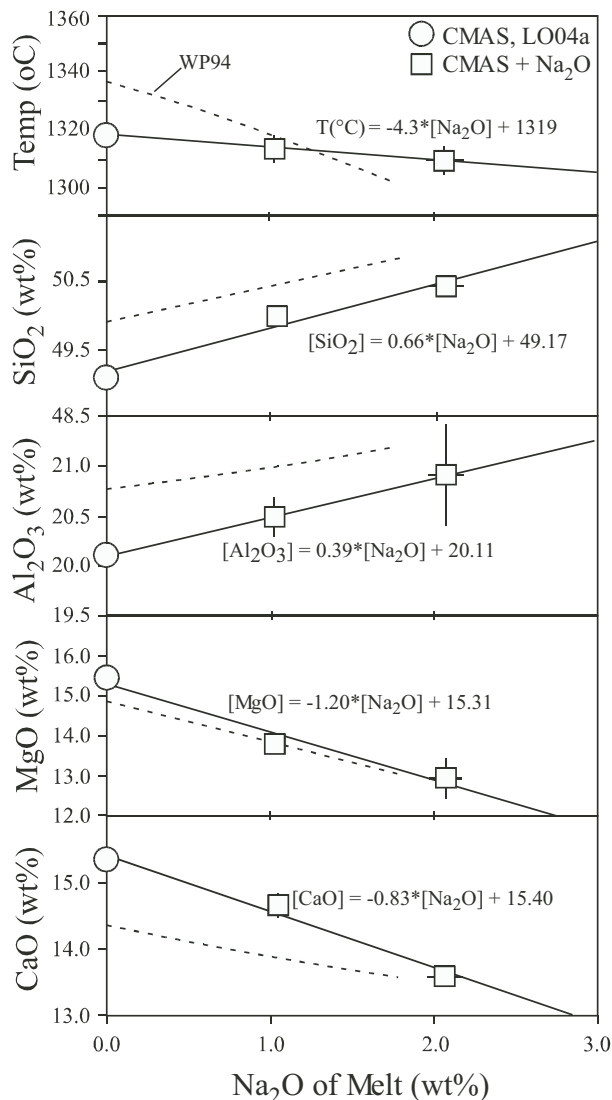
Fig. 6. A comparison diagram of the effects of Na$_2$O on the solidus and the melt composition at 1·1 GPa between this study and Walter & Presnall (1994), labelled WP94 and plotted as dashed lines. The data for the isobarically invariant point of the Sp-lherzolite in system CMAS at 1·1 GPa are from Liu & O'Neill (2004*a*), labelled LO04a.

we could subtract these effects from our results on the H$_2$O-containing experiments, to reveal the effects of H$_2$O alone. However, the obvious interaction between H$_2$O and CO$_2$ that we observed along the CO$_2$-rich part of the vapour saturation curve (Fig. 4; also King & Holloway, 2002) makes this oversimplified approach logically untenable. We have therefore addressed the problem by parameterizing empirically all our relevant data, including a term for H$_2$O–CO$_2$ interactions. We can then check to see whether the effects of CO$_2$ and Na$_2$O from our parameterization are the same as observed directly in the H$_2$O-free systems. If so, then this would be corroborative evidence that we have accounted for Na$_2$O and

CO$_2$ adequately. This approach is robust, insofar as the effects of H$_2$O are so much larger than those of Na$_2$O and CO$_2$.

We assumed the relationship

$$[X] = [X]_{CMAS} + A^X_{Na_2O}[Na_2O] + A^X_{H_2O}[H_2O]$$
$$+ A^X_{CO_2}[CO_2] + A^X_{H_2O/CO_2}[H_2O][CO_2] \quad (3)$$

where the parameter denoted $[X]$ is either temperature (T_{melt}) or melt composition, i.e. [SiO$_2$], [Al$_2$O$_3$], [CaO] and [MgO]. These latter oxide concentrations can be reported in two ways, either with all components including H$_2$O and CO$_2$ summing to 100 wt %, or with H$_2$O and CO$_2$ removed and the remaining components renormalized to 100 wt %. The second way is implicitly adopted when the results are plotted on a phase diagram, such as that of Fig. 5. It is also relevant when comparing with most analytical data on natural samples, except for those on glasses that have not degassed (which is probable for H$_2$O but most unlikely for CO$_2$; Stolper & Newman, 1994).

We fitted the experimental data (Tables 4 and 5) assuming the compositional uncertainties given in these tables, and an uncertainty in experimental temperature of ±5 degrees. Only melt compositions multiply saturated by Fo + Sp + Opx + Cpx + Melt ± Vapour were used, with the isobarically invariant melt composition at 1·1 GPa in the system CMAS from Liu & O'Neill (2004*a*) included. The experiments with disequilibrium high-Al$_2$O$_3$ Opx or Cpx (C-1838, C-1878, C-1889 and C-1882) were excluded, and also one experiment (C-1893) with anomalous melt composition. The total number of data in the final regression is 28. We assumed that the contents of H$_2$O and CO$_2$ in the melts in C-1780 and C-1773 and in the isobarically invariant melt from Liu & O'Neill (2004*a*) to be 0·05 ± 0·05 wt %. The coefficients for the regressions are given in Table 6, along with the reduced chi-squared (χ^2_v) statistic.

The effect of small amounts of Na$_2$O on the solidus temperature derived from the regression is −4·2°C/wt %, in excellent agreement with the result determined directly from our experiments in the system CMAS ± Na$_2$O (Fig. 6). This agreement indicates that the effect of small amounts of Na$_2$O in our hydrous experiments can be successfully removed by the regression procedure. The effect of CO$_2$ on the partial melting temperature is −7°C/wt % CO$_2$, which predicts that the depression of the solidus caused by 0·6 wt % CO$_2$ dissolved in the H$_2$O-free system would be 4°C. This is too small to be observed directly, which is consistent with our experimental observations in CMAS–CO$_2$. The effect of H$_2$O on the solidus, ~45·4°C/wt %, is obviously very much larger.

The multiply saturated melt compositions obtained by extrapolating to 0% Na$_2$O and 0% CO$_2$ are plotted as a function of [H$_2$O] in Fig. 7. When oxide concentrations

are reported with [H_2O] included in the analytical total, increasing [H_2O] does not change [SiO_2] perceptibly, increases [Al_2O_3], but decreases [MgO] and [CaO]. The decrease in [MgO] and [CaO] was also observed by Gaetani & Grove (1998) in natural rock composition systems, but their experiments suggested that [SiO_2] decreases whereas [Al_2O_3] was more or less unaffected.

When melt compositions are renormalized to a volatile-free basis (Fig. 7), however, our results translate into an increase of [SiO_2] with added [H_2O], [MgO] and [CaO] still decrease.

Interaction of H_2O and CO_2

A remarkable observation of this study is the strong interaction between H_2O and CO_2 (Table 6, Figs 8 and 9). Specifically, the partial melting temperature is increased by 16 degrees for one unit increase of [H_2O][CO_2] ($\%^2$ by weight). As regards melt compositions, SiO_2 is changed by -0.32 wt %, Al_2O_3 by -0.66 wt %, MgO by 0.95 wt % and CaO by 0.24 wt % for one unit increase of [H_2O][CO_2]. When we consider the term [H_2O][CO_2] with the term [CO_2] together, the general effects of CO_2 on the melt compositions of the system CMAS + H_2O are decreasing SiO_2 and Al_2O_3, but increasing MgO and CaO (Fig. 9), in agreement with the observation made by Hirose (1997b) on the partial melting of the carbonated peridotite KLB-1. As a result of the interaction between H_2O and CO_2, the effects of a small amount of CO_2 on both the multiply saturated melt composition and T_{melt} are almost negligible at H_2O-poor conditions, but become important at H_2O-rich conditions. It should be noted that the effects of CO_2 on the multiply saturated melt composition are generally opposite to the effects of H_2O.

It is well known that H_2O depolymerizes silicate melts whereas CO_2 does the reverse (e.g. Mysen & Virgo, 1980). When CO_2 is present, more H_2O is required to depolymerize the silicate melt to a certain degree of polymerization to counteract the effect of CO_2, and vice versa.

Using the regression coefficients in Table 6, we have calculated the melt compositions from 0% to 3·5% H_2O at both 0% CO_2 and 0·6% CO_2. The calculated melt compositions are shown in Fig. 10a and b. When the system is H_2O-free and CO_2-free, the product melt of Sp-lherzolite at 1·1 GPa is essentially olivine basalt (Presnall et al., 1979; Walter & Presnall, 1994; Liu & O'Neill, 2004a). As water is added, Al_2O_3 increases so that melts become richer in normative An, leaving less CaO to form Di. Because CaO also decreases by the addition of H_2O, normative Di decreases rapidly (Fig. 10a). Because H_2O does not affect the SiO_2 content but decreases the MgO content, melts become richer in normative Hy, reaching the quartz-normative line at

Table 6: Multiply saturated melt compositions in the system CMAS $\pm$ Na_2O $\pm$ H_2O $\pm$ CO_2: results of multiple non-linear least-squares regression [equation (3) in the text]

Variable	Constant	[Na_2O]	[H_2O]	[CO_2]	[H_2O][CO_2]	χ_v^2
T	1319	−4·2	−45·4	−7·0	16·0	2·9
[SiO_2]	49·30	0·47	—	−0·74	−0·32	1·8
[SiO_2]*	49·17	0·52	0·59	—	−0·48	1·8
[Al_2O_3]	19·81	0·48	0·72	—	−0·66	4·1
[Al_2O_3]*	19·80	0·44	0·86	—	−0·52	3·8
[MgO]	16·13	−0·98	−1·37	−0·85	0·95	8·3
[MgO]*	16·14	−0·97	−1·29	−0·69	1·00	9·1
[CaO]	14·89	−0·65	−0·38	—	0·24	5·4
[CaO]*	14·96	−0·70	−0·26	—	0·31	5·5

*Oxides recalculated by normalizing [SiO_2] + [Al_2O_3] + [MgO] + [CaO] + [Na_2O] to 100% on a volatile-free basis.

~1·5% water. The quartz-normative character of hydrous mantle melts has of course long been appreciated (e.g. Kushiro, 1972).

The small amount of CO_2 (0·6 wt %) that dissolves in the multiply saturated melts at 1·1 GPa at H_2O-free conditions has negligible effects on melt composition. With 3·5 wt % H_2O, however, a similarly small amount of CO_2 noticeably modifies the multiply saturated melt composition (Fig. 10b): it increases the Di component of the melt (projection from Ol), while shifting the composition towards the AbAnOr–Ol plane (projection from Di). As is apparent in Fig. 10b, the effect of CO_2 on modifying the melt properties at H_2O-rich conditions is generally opposite to, but much larger than, that of H_2O. It follows that the shift of melt property caused by a large amount of H_2O can be counteracted by a small amount of CO_2.

## Melting reaction for Sp-lherzolite in the system CMAS + H_2O

The partial melting reaction for Sp-lherzolite in the system CMAS–H_2O at 1·1 GPa was calculated using the method of Walter et al. (1995); it should be noted that this reaction is independent of bulk composition in the simple system as long as all the phases are present. The reaction coefficients are illustrated in Fig. 11 as a function of temperature.

At anhydrous conditions (1319°C) Opx, Cpx and Sp react to produce Melt and Fo. With increasing H_2O and falling temperature the amount of Cpx consumed by the reaction decreases whereas that of Opx increases, such that below 1224°C Cpx is produced peritectically
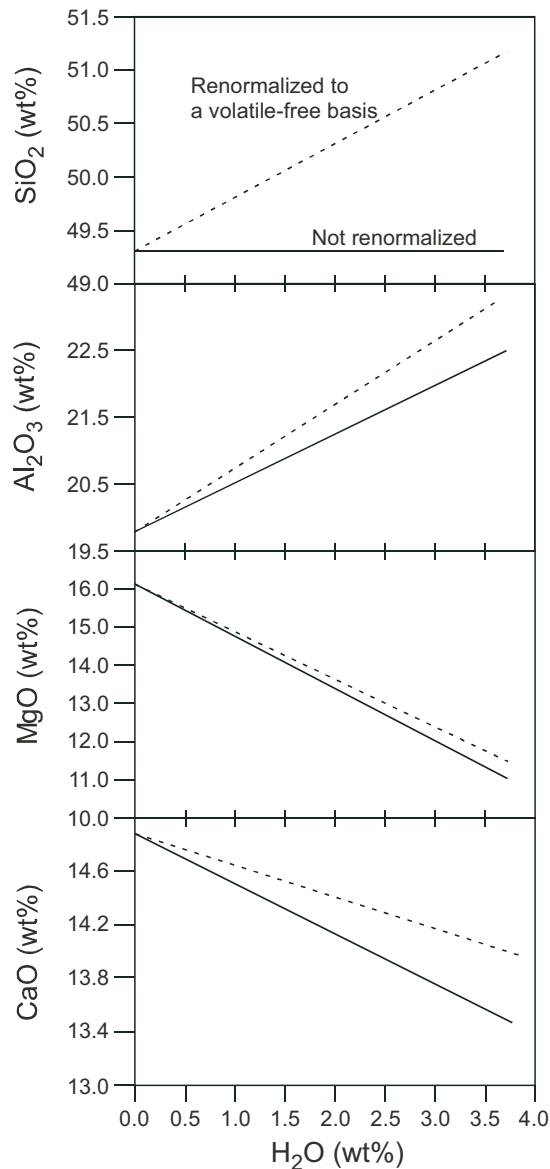
Fig. 7. The inferred effects of H_2O on the compositions of CO_2-free multiply saturated partial melts in CMAS–H_2O, obtained from fits of the experimental data to equation (3) in the text and extrapolating to $[CO_2] = 0$. The results are plotted in two ways: 'renormalized' (dashed lines) means that the amount of H_2O in the analytical totals is subtracted, and the analysis recalculated to sum to 100%; 'not renormalized' (continuous lines) means that the totals are summed to 100% including H_2O. (For the regression coefficients, see Table 6.)

$(Opx + Sp \rightarrow Melt + Fo + Cpx)$. This trend agrees with the reaction observed by Gaetani & Grove (1998) at $1\cdot2$ GPa and their calculated result at $1\cdot0$ GPa using the phase composition data of Hirose & Kawamoto (1995) for a natural peridotitic system. Loss of Opx before Cpx under hydrous conditions has been observed in several other studies (Green, 1973; Hirose, 1997a). Similar behaviour was found in the system CMAS–K_2O (Liu &
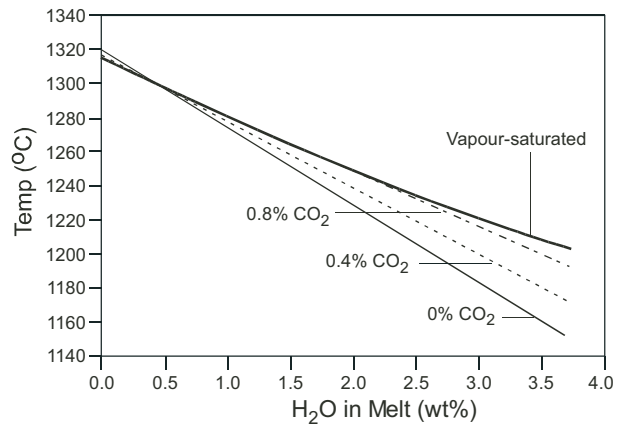
Fig. 8. The effect of H_2O on the temperature at which melt is multiply saturated with Fo + Sp + Opx + Cpx for different amounts of CO_2 (0, $0\cdot4$ and $0\cdot8$ wt % in the melt). The depression of the solidus as a function of H_2O in the melt along the CO_2-rich vapour-saturation curve is also indicated.

O'Neill, 2004a); interestingly, the effect of K_2O on peridotite melting is in many ways more akin to that of H_2O than to Na_2O.

Recognizing the reaction relationship between Melt and Fo + Cpx is critical to the evaluation of reversal crystallization experiments (the 'inverse approach'), as it means that a melt produced in equilibrium with Fo + Cpx will not crystallize these phases. Because the hydrous partial melting reactions were not accurately known before, the hydrous reversal crystallizing experiments in the literature, aiming at gathering source information of some igneous rocks, should be used with great caution (Nicholls & Ringwood, 1972, 1973; Mysen *et al.*, 1974; Green, 1976; Pichavant *et al.*, 2002).

The reaction relationship furthermore suggests that a possible mechanism for producing wehrlite in mantle sections might be by interaction with hydrous melts.

DISCUSSION
Hydrous partial melting of Sp-lherzolite in multicomponent (natural) compositions at ~1·1 GPa

Experiments on the partial melting of Sp-lherzolite with small amounts of H_2O using natural compositions have been undertaken by Hirose & Kawamoto (1995), Hirose (1997a) and Gaetani & Grove (1998); the key experiments at pressures near $1\cdot1$ GPa are summarized in Table 7, and plotted on the projection from Ol onto the plane Di–JdCaTsLc–Qz in Fig. 12. Superficially, there appears to be a considerable difference between one group of results, those of Hirose & Kawamoto (1995), Hirose (1997a) and
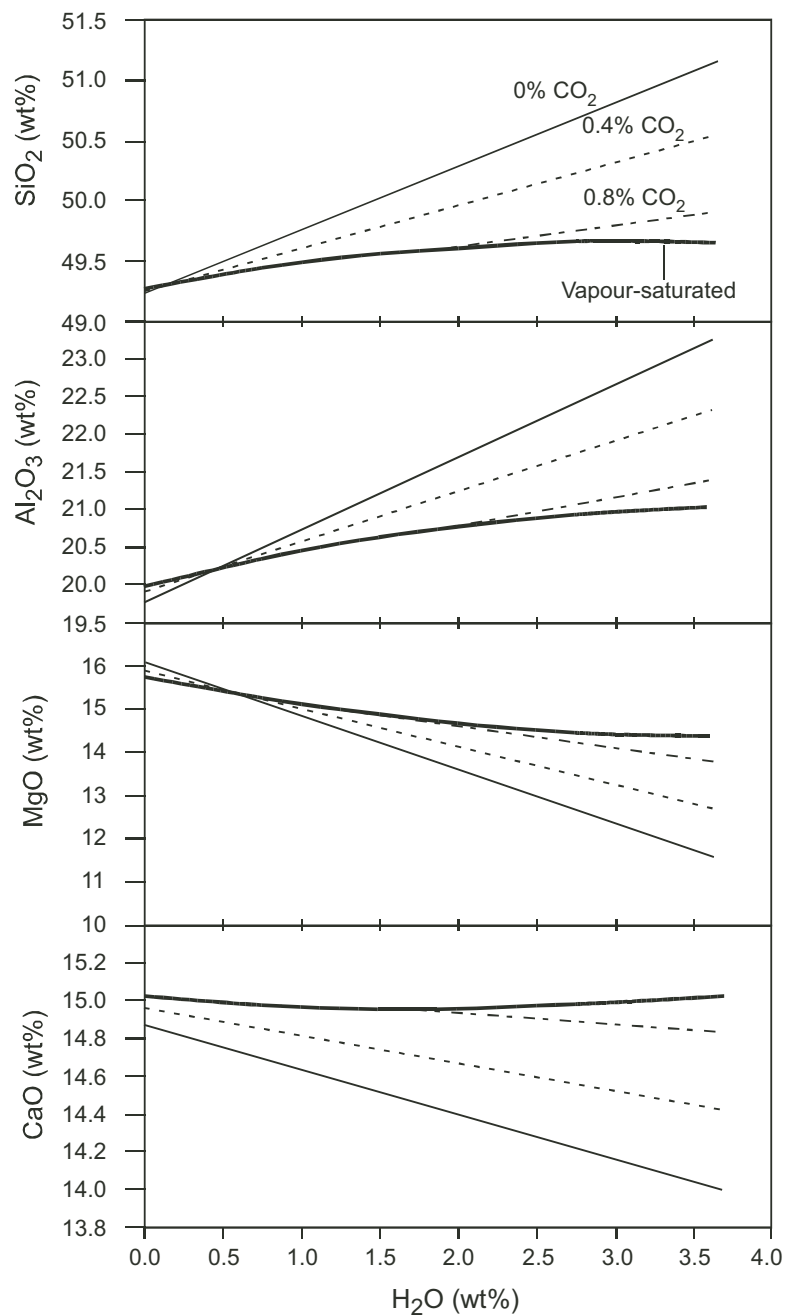
Fig. 9. Combined effects of H_2O and CO_2 on the multiply saturated melt compositions with small amounts of CO_2 (0, 0·4 and 0·8 wt %) in the melts. The melt compositions as a function of H_2O in the melt along the CO_2-rich vapour-saturation curve are also indicated.

this work, which find that increasing H_2O moves the melt composition away from the Di apex and towards the JdCaTsLc–Qz join, and the results of Gaetani & Grove (1998), from which the effect of H_2O on melt compositions appears negligible. We believe that our present results combined with previous work on the effects of adding individual components (FeO from Gudfinnsson & Presnall, 2000; Cr_2O_3 from Liu & O'Neill, 2004b) on

multiply saturated melting in CMAS can resolve these apparent discrepancies, and also integrate these hydrous partial melting results with the large body of work on anhydrous melting in natural, multicomponent peridotites. Our approach is to start with the isobaric invariant point in CMAS, which may be plotted unambiguously in the tetrahedron Ol–JdCaTsLc–Di–Qz, and examine the influence of other components (specifically,
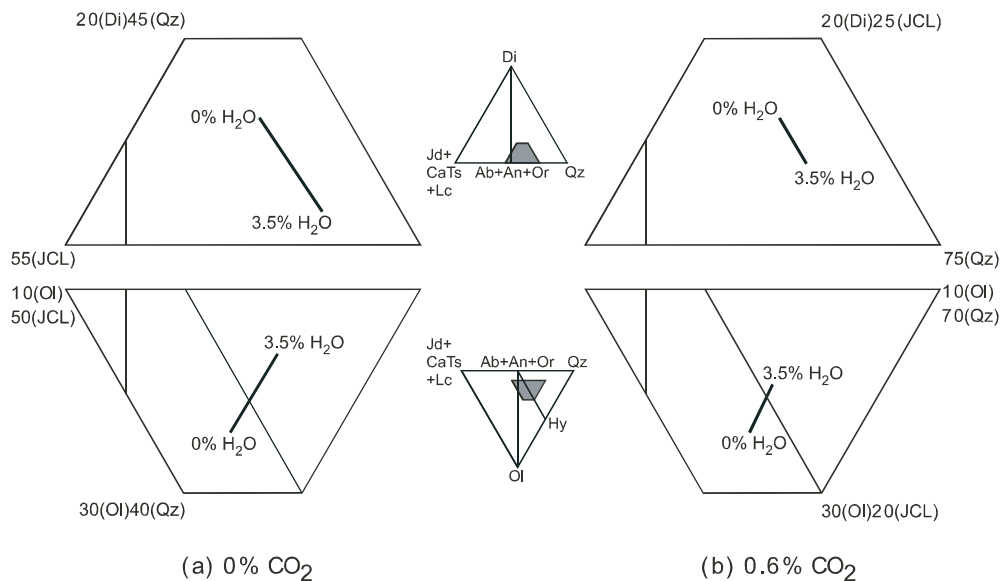
Fig. 10. Multiply saturated melt compositions at 1·1 GPa in the system CMAS–H₂O–CO₂ projected onto the planes Di–JdCaTsLc–Qz from Ol and Ol–JdCaTsLc–Qz from Di at (a) 0% CO₂, and (b) 0·6% CO₂. Comparison of the CO₂-free trend with that at 0·6 wt % CO₂ shows that the effect of CO₂ is to counteract partly that of H₂O.
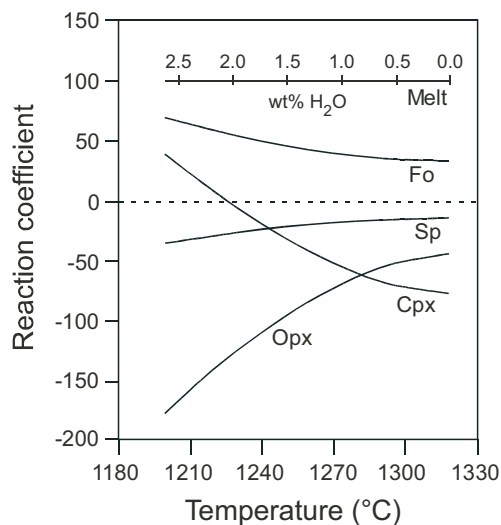
Fig. 11. Melting reaction of Sp-lherzolite in the system CMAS + H₂O at 1·1 GPa. Reaction coefficients have been normalized to 100 Melt. The wt % H₂O in the melt indicated.

Na₂O, FeO, Cr₂O₃, H₂O and CO₂) individually, using 'vectors' emanating from this invariant point, contoured in the amounts of the component. These 'vectors' are obtained from experiments in which the component of interest, or in the case of CO₂ and H₂O, a combination of the two components, is added to CMAS. Our approach assumes that the interactions between these non-CMAS components can be neglected, with the exception of the H₂O–CO₂ interaction emphasized in this study. We acknowledge that this is a questionable assumption, and

should be regarded only as a working hypothesis until more data are available.

In terms of weight percent oxide, the most abundant of the non-CMAS components in natural peridotite is FeO. However, the detailed work of Gudfinnsson & Presnall (2000) has established that this component has an almost negligible effect on the normative representation of multiply saturated melt compositions at ~1·1 GPa in the Ol–JdCaTsLc–Di–Qz tetrahedron, at concentrations appropriate for equilibrium with mantle olivine with mg-number of 90. Hence the FeO 'vector' hardly shows up on the projection of Fig. 12, and FeO has an insignificant effect on the following argument.

The compositional trend of anhydrous melting of natural peridotite at ~1·1 GPa is taken from Falloon *et al.* (1999), and is represented by the large grey arrow in Fig. 12. This arrow starts well to the left of the isobarically invariant point in CMAS, evidently because of the effect of Na₂O, as shown by the 'vector' for this component. Very low degree melts have high Na₂O concentrations, because this component is not buffered by the four-phase lherzolite assemblage and its incompatibility means that it is concentrated in the melt [for a fuller discussion of this effect, see Hirschmann *et al.* (1998) and Robinson *et al.* (1998)]. With increasing degree of melting, the Na₂O content of the melt decreases as a result of the dilution effect, whereas an increase in the $Cr_{\#}^{sp}$ coexisting spinel, which monitors the activity of Al₂O₃ (see Liu & O'Neill, 2004*b*), causes the trajectory to move upwards (towards the Di apex), as indicated by the $Cr_{\#}^{sp}$ 'vector'. The trend of the melt composition with increasing degree of melting of anhydrous mantle peridotite is thus

Table 7: Hydrous partial melting experiments on natural compositions at 1·0–1·5 GPa from the literature

Run	T (°C)	t (h)	Starting material	Capsule	Sleeve	Phases observed	% melt	wt % H_2O	wt % CO_2
Experiments at 1·0 GPa from Hirose & Kawamoto (1995)									
38	1200	65	KLB-1 + H_2O*	Au–Pd	Alsimag	Ol + Sp + Opx + Cpx + Melt	12·4	1·6† (1·6)‡	?
36	1100	65·6	KLB-1 + H_2O	Ag–Pd	Alsimag	Ol + Sp + Opx + Cpx + Melt	7·0	7·1§	?
37	1100	47·9	KLB-1 + H_2O	Ag–Pd	Alsimag	Ol + Sp + Opx + Cpx + Melt	13·4	6·9† (3·4)‡	?
Experiments at 1·0 GPa from Hirose (1997a)									
50	1050	72	KLB-1 + H_2O*	Au	Alsimag	Ol + Sp + Opx + Cpx + Melt	15·8	6·3†	?
51	1050	66·5	KLB-1 + H_2O	Au	Alsimag	Ol + Sp + Opx + Cpx + Melt + V(?)	22·1	?	?
Experiments at 1·2 GPa from Gaetani & Grove (1998)									
B303	1345	24	P + anhydrous-B§	Au–Pd¶	Graphite	Ol + Sp + Opx + Cpx + Melt	61·0	0·71**	?
B292	1330	24	P + anhydrous-B	Au–Pd¶	Graphite	Ol + Sp + Opx + Cpx + Melt	59·5	?	?
B287	1315	24	P + anhydrous-B	Au–Pd¶	Graphite	Ol + Sp + Opx + Cpx + Melt	58·6	0·98**	0·07**
B333	1245	25	P + hydrous-B	Au–Pd¶	Graphite	Ol + Sp + Opx + Cpx + Melt	68·7	(3·3)‡	?
B305	1230	24	P + hydrous-B	Au–Pd¶	Graphite	Ol + Sp + Opx + Melt	74·7	4·5**	1·27**
B304	1215	24	P + hydrous-B	Au–Pd¶	Graphite	Ol + Sp + Opx + Cpx + Melt	68·6	(5·99)‡	?
B330	1200	29	P + hydrous-B	Au–Pd¶	Graphite	Ol + Sp + Opx + Cpx + Melt	71·2	(5·06)‡	?
B329	1185	26	P ± hydrous-B	Au–Pd¶	Graphite	Ol ± Sp ± Opx ± Cpx ± Melt	59·0	(6·26)‡	?

t, experimental time in hours; Sleeve, material of sleeve or powder surrounding the capsule. Water-loss from H_2O-rich experiments may have been severe, as indicated by Run 37 of Hirose & Kawamoto (1995). A substantial amount of CO_2 may have been present in the H_2O-rich experiments of Gaetani & Grove (1998), as indicated by their Run 305.
*Peridotite KLB-1 + distilled water. †Calculated by mass-balance. ‡Ion probe. §Peridotite + anhydrous or hydrous basalt. ¶Capsule presaturated in Fe using basaltic or andesitic glass. **FTIR.

explained, at least qualitatively, by the combined effects of the Na_2O and $Cr^{sp}_\#$ 'vectors'.

The multiply saturated melt compositions found by Hirose & Kawamoto (1995) and Hirose (1997a) with small amounts of H_2O are displaced from the anhydrous melting trend parallel to our H_2O 'vector', that is, in agreement with the effect of H_2O deduced in this study. We infer that these experiments may have escaped CO_2 contamination, as a result of the use of an Alsimag sleeve around the capsule. However, the melt compositions of Gaetani & Grove (1998) appear not to show the H_2O trend, but rather plot on the anhydrous trend of Falloon *et al.* (1999), at approximately the appropriate Na_2O (their experimental melts contain 2·06–2·5 wt % Na_2O, and are in equilibrium with spinel with $Cr^{sp}_\# = 0·05$–0·2). We suggest that this is caused by substantial amounts of CO_2 in their experiments, as indicated by their experiment B305 (Table 7), which contains 1·27 ± 0·14 wt % CO_2; this amount counteracts the effect of H_2O more or less completely in this projection, as shown in Fig. 12b and c by the shrinking of the H_2O 'vector'.

CONCLUSIONS

The effects of H_2O, CO_2 and Na_2O on partial melting of model Sp-lherzolite (Ol + Sp + Opx + Cpx) in the system CMAS has been studied at 1·1 GPa. The amount of H_2O in a melt has a strong effect on the temperature at which the melt coexists with the Sp-lherzolite assemblage: 1 wt % H_2O depresses temperature by ~45 degrees. The effect of CO_2 by itself is relatively minor, as 1 wt % CO_2 depresses temperature by only ~7 degrees, and the saturation level of CO_2 in the melt is only 0·6 wt %. However, when H_2O is present, the effect of CO_2 becomes much more significant, as one unit of $[H_2O]$ $[CO_2]$ (in wt %²), increases the melting temperature by 16 degrees.

A relatively small amount of H_2O in the melt can significantly affect the multiply saturated melt compositions: 1 wt % H_2O decreases MgO by 1·37 wt % and CaO by 0·38 wt %, increases Al_2O_3 by 0·72 wt %, but leaves SiO_2 constant (calculated on the basis that all components including H_2O and CO_2 sum to 100 wt %). The effects of CO_2 on the melt compositions, which are generally opposite to those of H_2O, are minor at H_2O-free conditions but become more significant as H_2O increases, and may largely cancel out the effects of H_2O on the melt composition at saturation with CO_2-rich vapour. The strong interaction between CO_2 and H_2O in the melt also causes the solubility of CO_2 at vapour saturation to increase with increasing H_2O.

In terms of normative components, the multiply saturated melt in the anhydrous CMAS system is an olivine basalt. Increasing Na_2O drives the composition towards
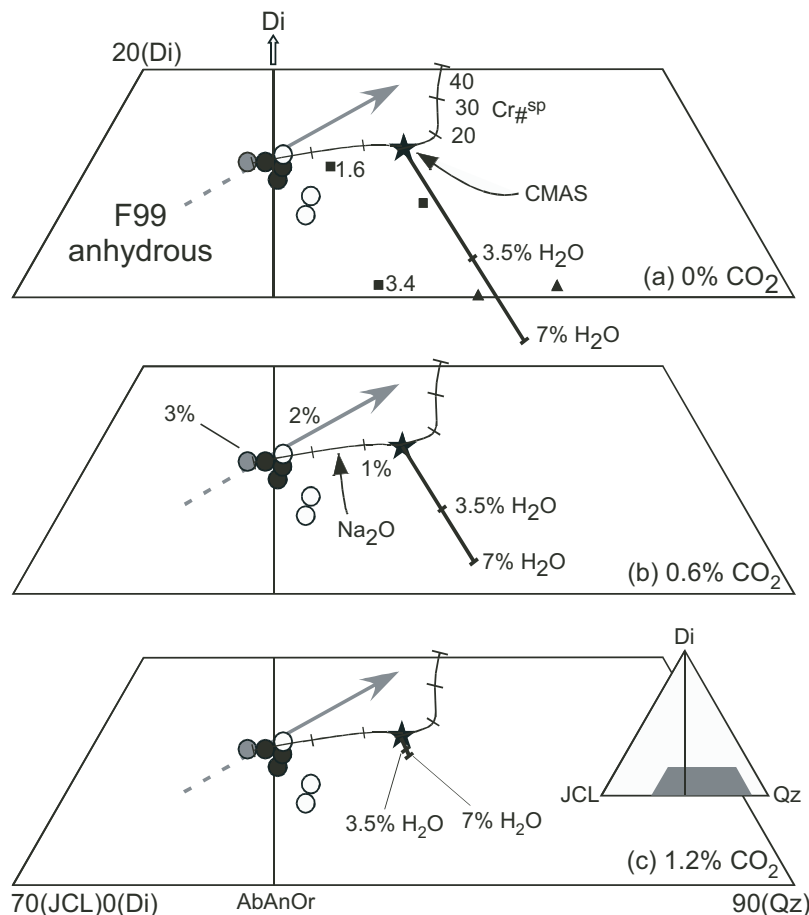
Fig. 12. Understanding the melting behaviour of natural compositions: deconvoluting the effects of Na_2O, H_2O, CO_2 and $Cr_\#^{sp}$ in multiply saturated melting of Sp-lherzolite at pressures near 1·1 GPa, shown on the plane Di–JdCaTsLc–Qz projected from Ol. To display better the effect of CO_2 in largely nullifying that of H_2O, three otherwise identical diagrams are drawn, for (a) 0% CO_2, (b) 0·6% CO_2, and (c) 1·2% CO_2. The composition of the isobarically invariant melt in the system CMAS at 1·1 GPa (filled star) is from Liu & O'Neill (2004*a*). The effect of Cr_2O_3 on the melt composition is from Liu & O'Neill (2004*b*), shown contoured using the molar Cr/(Cr + Al) of coexisting spinel ($Cr_\#^{sp}$). The trend of compositions of anhydrous melts produced by multiply saturated partial melting of natural mantle composition, from Falloon *et al.* (1999), at 1·0 GPa, is shown as the large grey arrow labelled F99 anhydrous; the direction of the arrow indicates increasing temperature, and the dashed part (at lower temperature) shows where melting is in the plagioclase lherzolite field, the solid part of the grey being in the Sp-lherzolite field. Melt compositions from Gaetani & Grove (1998) are shown as circles: ○, H_2O <1 wt %; grey circle, H_2O close to 3 wt %; ●, H_2O >5 wt % (up to 6·3 wt %). Also plotted in (a) are the data from Hirose & Kawamoto (1995; ■) and Hirose (1997*a*; ▲), with H_2O from ion probe measurements (in wt %) indicated.

becoming nepheline normative. The effect of Na_2O differs in this important respect from that of K_2O, the addition of which makes the melt more quartz-normative (Liu & O'Neill, 2004*a*). The effect of H_2O is somewhat similar to that of K_2O, and with increasing H_2O the melt becomes Qz-rich and Di-poor. With ~1·5 wt % H_2O in the melt, the melt is Qz-normative; with ~5 wt %, our parameterization predicts that the melt would be very Qz-rich and on the verge of becoming corundum-normative. Whether this actually happens requires further experimental investigation, which we emphasize will not be an easy task because of the low temperatures involved, quench modification of melt compositions, the likelihood of the CO_2 contamination that

plagued this study, and the fact that Pt capsules are largely open to H through this component's rapid diffusion. The latter two points indicate that any such study must include analysis of both H_2O and CO_2 in the melt.

ACKNOWLEDGEMENTS

REFERENCES

Asimow, P. D. & Langmuir, C. H. (2003). The importance of water to oceanic mantle melting regimes. *Nature* **421**, 815–820.

Baker, M. B. & Stolper, E. M. (1994). Determining the composition of high-pressure mantle melts using diamond aggregates. *Geochimica et Cosmochimica Acta* **58**, 2811–2827.

Behrens, H., Ohlhorst, S., Holtz, F. & Champenois, M. (2004). CO_2 solubility in dacitic melts equilibrated with $H_2O–CO_2$ fluids: implications for modelling the solubility of CO_2 in silicic melts. *Geochimica et Cosmochimica Acta* **68**, 4687–4703.

Blank, J. G. & Brooker, R. A. (1994). Experimental studies of carbon dioxide in silicate melts: solubility, speciation, and stable carbon isotope behaviour. In: Carroll, M. R. & Holloway, J. R. (eds) *Volatiles in Magmas. Mineralogical Society of America, Reviews in Mineralogy* **30**, 157–186.

Bose, K. & Ganguly, J. (1995). Quartz–coesite transition revisited: reversed experimental determination at 500–1200°C and retrieved thermochemical properties. *American Mineralogist* **80**, 231–238.

Bowen, N. L. (1928). The evolution of the igneous rocks. *Glass Technology* **16**, 20–24.

Boyd, F. R. & England, J. L. (1960). Apparatus for phase-equilibrium measurements at pressures up to 50 kbar and temperatures up to 1750°C. *Journal of Geophysical Research* **65**, 741–748.

Brey, G. P. & Köhler, T. (1990). Geothermobarometry in four-phase lherzolite II: new thermobarometers, and practical assessment of existing thermobarometers. *Journal of Petrology* **31**, 1353–1378.

Brooker, R., Holloway, J. R. & Hervig, R. (1998). Reduction in piston-cylinder experiments: the detection of carbon infiltration into platinum capsules. *American Mineralogist* **83**, 985–994.

Church, B. N. & Johnson, W. M. (1980). Calculation of the refractive index of silicate glasses from chemical composition. *Geological Society of America Bulletin* **91**, 619–625.

Dalton, J. A. & Presnall, D. C. (1998a). The continuum of primary carbonatitic–kimberlitic melt compositions in equilibrium with lherzolite: data from the system $CaO–MgO–Al_2O_3–SiO_2–CO_2$ at 6 GPa. *Journal of Petrology* **39**, 1953–1964.

Dalton, J. A. & Presnall, D. C. (1998b). Carbonatitic melts along the solidus of model lherzolite in the system $CaO–MgO–Al_2O_3–SiO_2–CO_2$ from 3 to 7 GPa. *Contributions to Mineralogy and Petrology* **131**, 123–135.

Dixon, J. E., Leist, L., Langmuir, C. & Schilling, J.-G. (2002). Recycled dehydrated lithosphere observed in plume-influenced mid-ocean-ridge basalt. *Nature* **420**, 385–389.

Eggler, D. H. (1978). The effect of CO_2 upon partial melting of peridotite in the system $Na_2O–CaO–Al_2O_3–MgO–SiO_2–CO_2$ to 35 kb, with an analysis of melting in a peridotite–$H_2O–CO_2$ system. *American Journal of Science* **278**, 305–343.

Eggler, D. H. & Wendlandt, R. F. (1979). Experimental studies on the relationship between kimberlite magmas and partial melting of peridotite. In: Boyd, F. R. & Meyer, H. O. A. (eds) *Kimberlites, Diatremes and Diamonds: their Geology, Petrology and Geochemistry. Proceedings of the Second International Kimberlite Conference, Volume 1*. Washington, DC: American Geophysical Union, pp. 330–338.

Falloon, T. J. & Danyushevsky, L. V. (2000). Melting of refractory mantle at 1·5, 2 and 2·5 GPa under anhydrous and H_2O-undersaturated conditions: implications for the petrogenesis of high-Ca boninites and the influences of subduction components on mantle melting. *Journal of Petrology* **41**, 257–283.

Falloon, T. J. & Green, D. H. (1988). Anhydrous partial melting of peridotite from 8 to 35 kbar and the petrogenesis of MORB. *Journal of Petrology, Special Issue* 379–414.

Falloon, T. J. & Green, D. H. (1989). The solidus of carbonated, fertile peridotite. *Earth and Planetary Science Letters* **94**, 364–370.

Falloon, T. J., Green, D. H., Danyushevsky, L. V. & Faul, U. H. (1999). Peridotite melting at 1·0 and 1·5 GPa: an experimental evaluation of techniques using diamond aggregates and mineral mixes for determination of near-solidus melts. *Journal of Petrology* **40**, 1343–1375.

Falloon, T. J., Danyushevsky, L. V. & Green, D. H. (2001). Peridotite melting at 1 GPa: reversal experiments on partial melt compositions produced by peridotite–basalt sandwich experiments. *Journal of Petrology* **42**, 2363–2390.

Fine, G. J. & Stolper, E. M. (1986). Dissolved carbon dioxide in basaltic glasses: concentrations and speciation. *Earth and Planetary Science Letters* **76**, 263–278.

Ford, C. E., Russell, D. G., Craven, J. A. & Fisk, M. R. (1983). Olivine–liquid equilibria: temperature, pressure and composition dependence of the crystal/liquid cation partition coefficients for Mg, Fe^{2+}, Ca and Mn. *Journal of Petrology* **24**, 256–265.

Gaetani, G. A. & Grove, T. L. (1998). The influence of water on melting of peridotite. *Contributions to Mineralogy and Petrology* **131**, 323–346.

Gasparik, T. (1984). Two-pyroxene thermobarometry with new experiment data in the system $CaO–MgO–Al_2O_3–SiO_2$. *Contributions to Mineralogy and Petrology* **87**, 87–97.

Genge, M. J., Jones, A. P. & Price, G. D. (1995). An infrared and Raman study of carbonate glasses: implications for the structure of carbonatite magmas. *Geochimica et Cosmochimica Acta* **59**, 927–937.

Gill, J. B. (1981). *Orogenic Andesite and Plate Tectonics*. New York: Springer.

Green, D. H. (1973). Experimental melting studies on a model upper mantle composition at high pressure under water-saturated and water-undersaturated conditions. *Earth and Planetary Science Letters* **19**, 37–53.

Green, D. H. (1976). Experimental testing of equilibrium partial melting of peridotite under saturated, high pressure conditions. *Canadian Mineralogist* **14**, 255–268.

Green, D. H. & Falloon, T. J. (1998). Pyrolite: a Ringwood concept and its current expression. In: Jackson, I. (ed.) *The Earth's Mantle: Composition, Structure and Evolution*. Cambridge: Cambridge University Press, pp. 311–378.

Green, D. H. & Wallace, M. E. (1988). Mantle metasomatism by ephemeral carbonatite melts. *Nature* **336**, 459–462.

Green, T. H., Ringwood, A. E. & Major, A. (1966). Friction effects and pressure calibration in a piston-cylinder high pressure–temperature apparatus. *Journal of Geophysical Research* **71**, 3589–3594.

Gudfinnsson, G. H. & Presnall, D. C. (2000). Melting behaviour of model lherzolite in the system $CaO–MgO–Al_2O_3–SiO_2–FeO$ at 0·7–2·8 GPa. *Journal of Petrology* **41**, 1241–1269.

Hibberson, W. O. (1978). High pressure and high temperature techniques as applied to experimental petrology. *Science and Technology* **15**(5), 22–23.

Hirose, K. (1997a). Melting experiments on lherzolite KLB-1 under hydrous conditions and generation of high-magnesian andesitic melts. *Geology* **25**, 42–44.

Hirose, K. (1997b). Partial melt compositions of carbonated peridotite at 3 GPa and role of CO_2 in the alkali-basalt magma generation. *Geophysical Research Letters* **24**(22), 2837–2840.

Hirose, K. & Kawamoto, T. (1995). Hydrous partial melting of lherzolite at 1 GPa: the effect of H$_2$O on the genesis of basaltic magmas. *Earth and Planetary Science Letters* **133**, 463–473.

Hirschmann, M. M., Baker, M. B. & Stolper, E. M. (1998). Effect of alkalis on silica contents of mantle-derived melts. *Geochimica et Cosmochimica Acta* **62**, 883–902.

Ihinger, P. D., Hervig, R. L. & McMillan, P. F. (1994). Analytical methods for volatiles in glasses. In: Carroll, M. R. & Holloway, J. R. (eds) *Volatiles in Magmas. Mineralogical Society of America, Reviews in Mineralogy* **30**, 67–121.

Ingerson, E. (1960). The water content of primitive granitic magma. *American Mineralogist* **35**, 806–815.

Jambon, A. (1994). Earth degassing and large-scale geochemical cycling of volatile elements. In: Carroll, M. R. & Holloway, J. R. (eds) *Volatiles in Magmas. Mineralogical Society of America, Reviews in Mineralogy* **30**, 479–517.

Jochum, K. P., Dingwell, D. B., Rocholl, A., Stoll, B., Hofmann, A. W., Becker, S., *et al.* (2000). The preparation and preliminary characterisation of eight geological MPI-DING reference glasses for *in situ* microanalysis. *Journal of Geostandards and Geoanalysis* **24**, 87–133.

Johannes, W., Bell, P. M., Mao, H. K., Boettcher, A. L., Chipman, D. W., Hays, J. F., Newont, R. C. & Seifert, F. (1971). An interlaboratory comparison of piston-cylinder pressure calibration using albite-breakdown reaction. *Contributions to Mineralogy and Petrology* **32**, 24–38.

King, P. L. & Holloway, J. R. (2002). CO$_2$ solubility and speciation in intermediate (andesitic) melts: the role of H$_2$O and composition. *Geochimica et Cosmochimica Acta* **66**, 1627–1640.

King, P. L., Vennemann, T. W., Holloway, J. R., Hervig, R. L., Lowenstern, J. B. & Forneris, J. F. (2002). Analytical techniques for volatiles: a case study using intermediate (andesitic) glasses. *American Mineralogist* **87**, 1077–1089.

Klemme, S. & O'Neill, H. St. C. (1997). The reaction MgCr$_2$O$_4$ + SiO$_2$ = Cr$_2$O$_3$ + MgSiO$_3$ and the free energy of formation of magnesiochromite (MgCr$_2$O$_4$). *Contributions to Mineralogy and Petrology* **130**, 59–65.

Köhler, T. & Brey, G. P. (1990). Calcium exchange between olivine and clinopyroxene calibrated as a geothermometer for natural peridotites from 2 to 60 kb with applications. *Geochimica et Cosmochimica Acta* **54**, 2375–2388.

Kushiro, I. (1969). The system forsterite–diopside–silica with and without water at high pressures. *American Journal of Science* **267A**, 269–294.

Kushiro, I. (1972). Effect of water on the composition of magmas formed at high pressures. *Journal of Petrology* **13**, 311–334.

Kushiro, I. (1975). On the nature of silicate melt and its significance in magma genesis: regularities in the shift of the liquids boundaries involving olivine, pyroxene, and silica minerals. *American Journal of Science* **272**, 411–431.

Kushiro, I. (1990). Partial melting of mantle wedge and evolution of island arc crust. *Journal of Geophysical Research* **95**, 15929–15939.

Kushiro, I., Yoder, H. S. & Nishikawa, M. (1968a). Effect of water on the melting of enstatite. *Geological Society of America Bulletin* **79**, 1685–1692.

Kushiro, I., Syono, Y. & Akimoo, S. (1968b). Melting of a peridotite nodule at high pressures and high water pressures. *Journal of Geophysical Research* **73**, 6023–6029.

Kushiro, I., Shimizu, N., Nakamura, Y. & Akimoto, S. (1972). Compositions of coexisting liquid and solid phases formed upon melting of natural garnet and spinel lherzolites at high pressures: a preliminary report. *Earth and Planetary Science Letters* **14**, 19–25.

Libourel, G. (1999). Systematics of calcium partitioning between olivine and silicate melt: implications for melt structure and calcium content

of magmatic olivines. *Contributions to Mineralogy and Petrology* **136**, 63–80.

Liu, T. C. & Presnall, D. C. (1990). Liquidus phase relationships on the join anorthite–forsterite–quartz at 20 kbar with applications to basalt petrogenesis and igneous sapphirine. *Contributions to Mineralogy and Petrology* **104**, 735–742.

Liu, X. & O'Neill, H. St. C. (2004a). Partial melting of spinel lherzolite in the system CaO–MgO–Al$_2$O$_3$–SiO$_2$ ± K$_2$O at 1·1 GPa. *Journal of Petrology* **45**, 1339–1368.

Liu, X. & O'Neill, H. St. C (2004b). The effect of Cr$_2$O$_3$ on the partial melting of spinel lherzolite in the system CaO–MgO–Al$_2$O$_3$–SiO$_2$–Cr$_2$O$_3$ at 1·1 GPa. *Journal of Petrology* **45**, 2261–2286.

McMillan, P. F. (1994). Water solubility and speciation models. In: Carroll, M. R. & Holloway, J. R. (eds) *Volatiles in Magmas. Mineralogical Society of America, Reviews in Mineralogy* **30**, 131–156.

Muntener, O., Kelemen, P. B. & Grove, T. L. (2001). The role of H$_2$O during crystallization of primitive arc magmas under uppermost mantle condition and genesis of igneous pyroxenites: an experimental study. *Contributions to Mineralogy and Petrology* **141**, 643–658.

Mysen, B. O. (1976). The role of volatiles in silicate melts: solubility of carbon dioxide and water in feldspar, pyroxene, and feldspathoid melts to 30 kb and 1625°C. *American Journal of Science* **276**, 969–996.

Mysen, B. O. & Boettcher, A. L. (1975a). Melting of a hydrous mantle. I. Phase relations of natural peridotite at high *P* and *T* and with controlled addition of water, carbon dioxide and hydrogen. *Journal of Petrology* **16**, 520–548.

Mysen, B. O. & Boettcher, A. L. (1975b). Melting of a hydrous mantle. II. Geochemistry of crystals and liquids formed by anatexis of mantle peridotite at high pressure and high temperature as a function of controlled activities of water, hydrogen and carbon dioxide. *Journal of Petrology* **16**, 549–593.

Mysen, B.O. & Virgo, D. (1980). Solubility mechanisms of carbon dioxide in silicate melts: a Raman spectroscopic study. *American Mineralogist*, **65**, 885–899.

Mysen, B. O., Kushiro, I., Nicholls, I. A. & Ringwood, A. E. (1974). A possible mantle origin for andesitic magmas: discussion of a paper by Nicholls and Ringwood. *Earth and Planetary Science Letters* **21**, 221–229.

Mysen, B. O., Eggler, D. H., Seitz, M. G. & Holloway, J. R. (1976). Carbon dioxide in melts of andesite, tholeiite, and olivine nephelinite composition to 30 kb pressure. *Contributions to Mineralogy and Petrology* **53**, 227–239.

Nicholls, I. A. & Ringwood, A. E. (1972). Production of silicate-saturated tholeiitic magmas in island arcs. *Earth and Planetary Science Letters* **17**, 243–246.

Nicholls, I. A. & Ringwood, A. E. (1973). Effect of water on olivine stability in tholeiites and production of silica-saturated magmas in the island arc environment. *Journal of Geology* **81**, 285–306.

Nickel, K. G., Brey, G. P. & Kogarto, L. (1985). Orthopyroxene–clinopyroxene equilibria in the system CaO–MgO–Al$_2$O$_3$–SiO$_2$. *Contributions to Mineralogy and Petrology* **91**, 44–53.

O'Hara, M. J. (1965). Primary magmas and the origin of basalts. *Scottish Journal of Geology* **1**, 19–40.

O'Neill, H. St. C. & Palme, H. (1998). Compositions of the Silicate Earth: implications for accretion and core formation. In: Jackson, I. (ed.) *The Earth's Mantle: Composition, Structure and Evolution.* Cambridge: Cambridge University Press, pp. 3–126.

Pan, V., Holloway, J. R. & Hervig, R. L. (1991). The pressure and temperature dependence of carbon dioxide solubility in tholeiitic basalt melts. *Geochimica et Cosmochimica Acta* **55**, 1587–1595.

Parman, S. W. & Grove, T. L. (2004). Harzburgite melting with and without H$_2$O: experimental data and predictive modelling. *Journal of Geophysical Research* **109**, B02201.

Pawley, A. R., Holloway, J. R. & McMillan, P. F. (1992). The effect of oxygen fugacity on the solubility of carbon–oxygen fluids in basaltic melt. *Earth and Planetary Science Letters* **110**, 213–225.

Pichavant, M., Mysen, B. O. & Macdonald, R. (2002). Source and H_2O content of high-MgO magmas in island arc settings: an experimental study of a primary calc-alkaline basalt from St. Vincent, Lesser Antilles arc. *Geochimica et Cosmochimica Acta* **66**, 2193–2209.

Presnall, D. C. (1976). Alumina content of enstatite as a geobarometer for plagioclase and spinel lherzolites. *American Mineralogist* **61**, 582–588.

Presnall, D. C., Dixon, S. A., Dixon, J. R., O'Donnell, T. H., Brenner, N. L., Schrock, R. L. & Dycus, D. W. (1978). Liquidus phase relations on the joint diopside–forsterite–anorthite from 1 atm. to 20 kbar: their bearing on the generation and crystallization of basaltic magma. *Contributions to Mineralogy and Petrology* **66**, 203–220.

Presnall, D. C., Dixon, J. R., O'Donnell, T. H. & Dixon, S. A. (1979). Generation of mid-ocean ridge tholeiites. *Journal of Petrology* **20**, 3–36.

Ringwood, A. E. (1975). *Composition and Petrology of the Earth's Mantle.* New York: McGraw–Hill.

Ringwood, A. E., Kesson, S. E., Hibberson, W. & Ware, N. (1992). Origin of kimberlites and related magmas. *Earth and Planetary Science Letters* **113**, 1746–1782.

Robinson, J. A. C., Wood, B. J. & Blundy, J. D. (1998). The beginning of melting of fertile and depleted peridotite at 1·5 GPa. *Earth and Planetary Science Letters* **155**, 97–111.

Schmidt, M. W. & Poli, S. (1998). Experimentally based water budgets for dehydrating slabs and consequences for arc magma generation. *Earth and Planetary Science Letters* **163**, 361–379.

Sen, G. (1985). Experimental determination of pyroxene compositions in the system $CaO–MgO–Al_2O_3–SiO_2$ at 900–1200°C and 10–15 kbar using PbO and H_2O fluxes. *American Mineralogist* **70**, 678–695.

Sen, G. & Presnall, D. C. (1984). Liquidus phase relationships on the join anorthite–forsterite–quartz at 10 kbar with applications to basalt petrogenesis. *Contributions to Mineralogy and Petrology* **85**, 404–408.

Stolper, E. M. (1982*a*). The speciation of water in silicate melts. *Geochimica et Cosmochimica Acta* **46**, 2609–2620.

Stolper, E. M. (1982*b*). Water in silicate glasses: an infrared spectroscopic study. *Contributions to Mineralogy and Petrology* **81**, 1–17.

Stolper, E. M. & Holloway, J. R. (1988). Experimental determination of the solubility of carbon dioxide in molten basalt at low pressure. *Earth and Planetary Science Letters* **87**, 397–408.

Stolper, E. M. & Newman, S. (1994). The role of water in the petrogenesis of Mariana trough magmas. *Earth and Planetary Science Letters* **121**, 293–325.

Taylor, W. R. & Green, D. H. (1988). Measurement of reduced peridotite–C–O–H solidus and implications for redox melting of the mantle. *Nature* **332**, 239–352.

Taylor, W. R. & Green, D. H. (1989). The role of reduced C–O–H fluids in mantle partial melting. In: Ross, J. (ed.) *Kimberlites and Related Rocks—Their Occurrence, Origin and Emplacement 1*. Carlton: Geological Society of Australia, pp. 592–602.

Ulmer, P. (2001). Partial melting in the mantle wedge—the role of H_2O in the genesis of mantle-derived 'arc-related' magmas. *Physics of the Earth and Planetary Interiors* **127**, 215–232.

Wallace, M. E. & Green, D. H. (1988). An experimental determination of primary carbonatite magma composition. *Nature* **335**, 343–346.

Walter, M. J. & Presnall, D. C. (1994). Melting behaviour of simplified lherzolite in the system $CaO–MgO–Al_2O_3–Na_2O$ from 7 to 35 kbar. *Journal of Petrology* **35**, 329–359.

Walter, M. J., Sisson, T. W. & Presnall, D. C. (1995). A mass proportion method for calculating melting reactions and application to melting of model upper mantle lherzolite. *Earth and Planetary Science Letters* **135**, 77–90.

Ware, N. G. (1991). Combined energy-dispersive–wavelength-dispersive quantitative electron microprobe analysis. *X-ray Spectrometry* **20**, 73–79.

Warner, R. D. (1973). Liquidus relations in the system $CaO–MgO–SiO_2–H_2O$ at 10 kb PH_2O and their petrologic significance. *American Journal of Sciences* **273**, 925–946.

Wasylenki, L. E., Baker, M. B., Kent, A. J. R. & Stolper E. M. (2003). Near-solidus melting of the shallow upper mantle: partial melting experiments on depleted peridotite. *Journal of Petrology* **44**, 1163–1191.

Wilson, M. (1989). *Igneous Petrogenesis.* London: Unwin Hyman.

Wohletz, K. (1996). Magma2: an estimation of magma physical and chemical properties with IUGG classification. Los Alamos National Laboratory, NM. http://www.ees1.lanl.gov/wohletz/Magma.htm/

Wyllie, P. J. (1977). Mantle fluid compositions buffered by carbonates in peridotite–CO_2–H_2O. *Journal of Geology* **85**, 187–207.

Wyllie, P. J. & Huang, W. L. (1975). Influence of mantle CO_2 in the generation of carbonatites and kimberlites. *Nature* **257**, 297–299.

Wyllie, P. J. & Huang, W. L. (1976). Carbonation and melting reactions in the system $CaO–MgO–SiO_2–CO_2$ at mantle pressures with geophysical and petrological applications. *Contributions to Mineralogy and Petrology* **54**, 79–107.

Yoder, H. S. (1971). The join diopside–pyrope–H_2O at 10 kb: its bearing on the melting of peridotite, the ACF metamorphic facies, and the gedrite–hornblende miscibility gap. *Carnegie Institute of Washington Yearbook* **69**, 176–181.

Yoder, H. S. & Tilley, C. E. (1962). Origin of basalt magmas: an experimental study of natural and synthetic rock systems. *Journal of Petrology* **3**, 342–532.

Zarubin, D. P. (1999). Infrared spectra of hydrogen bonded hydroxyl groups in silicate glasses. A re-interpretation. *Physics and Chemistry of Glasses* **40**, 184–192.

Zhang, Y. & Zindler, A. (1993). Distribution and evolution of carbon and nitrogen in Earth. *Earth and Planetary Science Letters* **117**, 331–345.